NATIONAL ADVISORY COMMITTEE FOR AERONAUTICS

TECHNICAL NOTE 3046

THEORETICAL CALCULATIONS OF THE EFFECTS OF FINITE SIDESLIP AT SUPERSONIC SPEEDS ON THE SPAN LOADING AND ROLLING MOMENT FOR FAMILIES OF THIN SWEPTBACK TAPERED WINGS AT AN ANGLE OF ATTACK

By Windsor L. Sherman and Kenneth Margolis

Langley Aeronautical Laboratory
Langley Field, Va.

Washington

November 1953

1K

NATIONAL ADVISORY COMMITTEE FOR AERONAUTICS

TECHNICAL NOTE 3046

THEORETICAL CALCULATIONS OF THE EFFECTS OF FINITE SIDESLIP AT SUPERSONIC SPEEDS ON THE SPAN LOADING AND ROLLING MOMENT FOR FAMILIES OF THIN SWEPTBACK TAPERED WINGS AT AN ANGLE OF ATTACK

By Windsor L. Sherman and Kenneth Margolis

SUMMARY

The material given in this report completes the presentation of results obtained from a general investigation of the effects of sideslip on the aerodynamic characteristics of thin sweptback tapered wings with side edges parallel to the axis of wing symmetry, the major phase of which was reported in NACA Technical Note 2898. By means of expressions derived therein, span load distributions have been calculated for several families of wings sideslipping at an angle of attack. Three basic combinations of Mach number and plan form have been investigated, each being subject to the conditions that the wing tips are parallel to the axis of wing symmetry and the trailing edge is supersonic, and to one of the following leading-edge conditions: (a) both leading edges subsonic, (b) one leading edge subsonic and one leading edge supersonic, and (c) both leading edges supersonic. In addition to the usual limitations of linear theory and the Mach number restriction imposed by the supersonic-trailing-edge condition, the restriction that the Mach line from the leading edge of the wing tip may not intersect the opposite half-wing has been imposed. The rolling-moment coefficient C_l and the corresponding stability derivative C_{l_β} have also been determined for wings with type (b) and (c) leading edges.

Results are given in the form of charts which present the span load distribution for values of sideslip angle up to 10°. Variations of the rolling-moment coefficient C_l with sideslip angle and of the stability derivative C_{l_β} with Mach number are also presented.

INTRODUCTION

A knowledge of the spanwise load distribution is of importance for both aerodynamic calculations and structural considerations in order

that the aerodynamic characteristics of the wing may be determined and the structural integrity of the airframe assured.

References 1 and 2 present detailed charts of span load distributions due to various wing motions for sweptback tapered wings with side edges parallel to the axis of wing symmetry (therein termed streamwise tips). The motions considered corresponded to constant angle of attack, steady rolling velocity, steady pitching velocity, and constant vertical acceleration. Reference 1 considers all four motions for wings with subsonic leading edges and supersonic trailing edges, while reference 2 treats the first three for wings having supersonic leading and trailing edges. The present paper contributes the span loading due to finite sideslip for this same general class of wings. The wings are sideslipping at an angle of attack and may be divided into three groups: (a) both leading edges subsonic, (b) one leading edge subsonic and one leading edge supersonic, and (c) both leading edges supersonic. The main restriction on the permissible combinations of Mach number and plan form is that the trailing edge is supersonic. A minor restriction is that the Mach line from the leading edge of the wing tip may not intersect the opposite half-wing.

The material given in this report completes the presentation of results obtained from a general investigation of the effects of sideslip on the aerodynamic characteristics of thin sweptback tapered wings with side edges parallel to the axis of wing symmetry, the major and basic phase of which was reported in reference 3. The span loadings for wings with both leading edges subsonic were computed by means of the load-distribution equations derived in reference 3. The span loadings for the other types of wings considered (i.e., those with one or both leading edges supersonic) were obtained by a numerical integration of the pressure-distribution equations presented in reference 3. This work, as well as the additional numerical integrations required to obtain the rolling moments, was performed by the National Bureau of Standards Computing Laboratory on the SEAC (Standards' Eastern Automatic Computer) which is a digital-type computer.

Results of the investigation are presented in the form of charts for the span load distribution for various values of Mach number, sideslip angle, and geometric parameters. Corresponding variations of the rolling-moment coefficient with sideslip angle and of the stability derivative C_{l_β} with Mach number are also shown. For purposes of completeness, results for the case of both leading edges subsonic previously reported in or obtainable from reference 3 have been included.

SYMBOLS

x,y	Cartesian coordinates (see fig. 1)
V	free-stream velocity
ρ	density of air
M	free-stream Mach number, V/Speed of sound
ΔC_p	coefficient of pressure difference between upper and lower surfaces of wing, positive in the sense of lift
b	wing span
c_r	wing root chord
c_y	local wing chord
c_{av}	average wing chord, S/b
S	wing area
A	aspect ratio, b^2/S
λ	taper ratio, Tip chord/Root chord
Λ	sweepback angle of leading edge
ϵ	semiapex angle, $\frac{\pi}{2} - \Lambda$
L	lift
C_L	lift coefficient, $L/\frac{1}{2}\rho V^2 S$
c_l	section lift coefficient
α	angle of attack
C_{L_α}	lift-curve slope, $\left(\frac{\partial C_L}{\partial \alpha}\right)_{\alpha \to 0}$
L'	rolling moment
C_l	rolling-moment coefficient, $L'/\frac{1}{2}\rho V^2 Sb$; positive direction of moment indicated in figure 1

β angle of sideslip; positive as shown in figure 1

$$C_{l_\beta} = \left(\frac{\partial C_l}{\partial \beta}\right)_{\beta \to 0}$$

Subscripts:

o evaluation for $\beta = 0$

TE trailing edge

LE leading edge

All angles are measured in radians unless otherwise indicated.

RESULTS AND DISCUSSION

The general plan form and the system of axes are shown in figure 1. There are three basic Mach line configurations considered; these are shown in figure 2. The wings will be referred to as type A (both leading edges subsonic); type B (one leading edge subsonic and one leading edge supersonic); and type C (both leading edges supersonic). The basic analysis used (ref. 3) is subject to the usual restrictions of linearized supersonic-flow theory as applied to uncambered wings having vanishingly small thickness. In addition to these restrictions there is a Mach number limitation imposed that requires the trailing edge to be supersonic. A minor limitation on the permissible configurations is that the Mach line from the leading edge of the tip may not intersect the opposite half-wing. Under the above-noted restrictions, the expressions for the span load distributions for type A wings and the pressure-distribution expressions for types A, B, and C wings were derived and presented in reference 3.

For type A wings the expressions given in reference 3 were used directly to compute the span loadings and rolling moments. Inasmuch as it was desired to "normalize" the span-load results for presentation in this paper, a multiplication factor $A/(C_{L_\alpha})_o$ was applied to the appropriate equations of reference 3. That is:

$$\frac{c_l c_y}{c_{av}(C_L)_o} = \frac{A}{(C_{L_\alpha})_o} \frac{c_l c_y}{b\alpha} \tag{1}$$

Values of $(C_{L_\alpha})_o$, the lift-curve slope for zero sideslip, required in equation (1) are obtainable from references 4 and 5.

For type B and C wings, the appropriate pressure-distribution equations given in reference 3 were set up on the SEAC computer and the pressure distribution determined at 19 points along the chord and for 60 spanwise locations. Numerical integrations were then carried out in order to obtain the span loading and rolling moment. These operations may be represented as follows:

$$\frac{c_l c_y}{c_{av}(C_L)_o} = \frac{A}{(C_{l_\alpha})_o b\alpha} \sum_{x_{LE}}^{x_{TE}} \Delta C_p \, \Delta x \tag{2}$$

and

$$\frac{C_l}{\alpha} = - \frac{1}{Sb} \sum_{-b/2}^{b/2} \left(\sum_{x_{LE}}^{x_{TE}} \Delta C_p \, \Delta x \right)_y \Delta y \tag{3}$$

(The minus sign in eq. (3) has been introduced to maintain the usual stability sign convention for C_l.)

Span load distributions for several sideslip angles (including $\beta = 0$ for reference) are presented in figures 3 to 8 for various combinations of aspect ratio, taper ratio, and leading-edge sweepback. For convenience, an index to these figures is given in table I. It should be noted that the span load distributions have been normalized with respect to the lift coefficient for the zero-sideslip condition. Consequently, for a given wing and Mach number, comparison of the integrated load distribution for $\beta = 0$ with that for a finite value of β gives a direct measurement of the change in lift due to sideslip.

Variations of the rolling-moment coefficient C_l with sideslip angle for several wings at various Mach numbers are presented in figures 9 to 12. Since some nonlinearities are known to occur in C_l (especially when edge conditions change), the points at which the values of C_l were calculated are indicated on the figures by an appropriate symbol. The dashed curves were faired through zero and these points. No symbols are shown at $\beta = 0$ since $C_l \equiv 0$ for $\beta = 0$.

Once the variation of the rolling-moment coefficient C_l is known, the stability derivative C_{l_β} can be obtained for type B and C wings in accordance with the following equation:

$$C_{l_\beta} = \left(\frac{\partial C_l}{\partial \beta}\right)_{\beta \to 0} \approx \left(\frac{\Delta C_l}{\Delta \beta}\right)_{\beta \to 0} \tag{4}$$

The values of C_{l_β} for type A wings are obtainable from the charts in reference 3.

Variations of the stability derivative C_{l_β} with Mach number are presented in figures 13 and 14 for wings of aspect ratio 2.0 and 4.0, respectively. As shown in reference 3, the values of C_{l_β} are negative for the Mach number range corresponding to subsonic-leading-edge conditions. As the Mach number increases, the value of C_{l_β} becomes less negative and for some wings actually changes sign and becomes positive in the supersonic-leading-edge range. (This effect is, of course, also evident from an examination of the curves for the rolling-moment coefficient presented in figs. 9 to 12.) In any event, an abrupt discontinuity is apparent (shown by dashed lines in figs. 13 and 14) at the Mach number corresponding to the sonic-leading-edge condition.

Some insight into this effect may be obtained by consideration from a theoretical viewpoint of the changes in wing loading that occur when the leading edge nearest the Mach cone changes from a subsonic to a supersonic condition. When this edge is subsonic, theoretically infinite pressures are concentrated along the edge. When the Mach number reaches the value for which the leading edge is sonic, the infinite pressures are replaced by finite pressures. The net effect of this sudden pressure change is not only to introduce a discontinuity in the slope of the rolling-moment curve, but also to reduce somewhat the absolute value of the rolling moment, that is, the resulting rolling moment is less negative. The pressure distribution over the entire wing surface is, of course, also changed; this change also contributes to the reduction of the absolute value of the rolling moment. In fact, for sweptback wings of taper ratio zero (no finite tip) the reduction in the absolute value of the rolling moment (that is, the increase in the positive direction) is always sufficient to cause a reversal in sign for C_{l_β}. (See results presented in ref. 6; note, however, that the results as presented therein indicate somewhat "modified" discontinuities.) When the wing has finite tips, such as those considered herein, the infinite pressures acting on the leading tip (which acts as a leading edge) persist even though one or both leading edges proper have become supersonic. Thus, for the finite-tip case one effect is still present which tends to maintain a negative rolling moment whereas the other effects discussed above tend to cause the rolling moment to change toward a positive value. The resulting total rolling moment is thus

dependent on the magnitudes of the opposing effects which are in turn dependent on the wing geometric parameters such as aspect ratio, taper ratio, and sweepback. The somewhat different results shown for the stability derivative C_{l_β} in figures 13 and 14, that is, reversal in sign of C_{l_β} for wings of aspect ratio 4.0 and lack of reversal for wings of aspect ratio 2.0, are therefore not inconsistent. In connection with figures 13 and 14, data for the subsonic-leading-edge cases have been included where possible (results taken from the charts of ref. 3). These data are easily identified; they are on the left-hand side (low Mach number range) of the dashed discontinuity line. For the higher Mach number range, calculated points are indicated by circles; the curves are faired through these values.

It should be noted that the values of C_{l_β} herein determined with respect to a body system of axes may be used directly in stability calculations without recourse to transformation formulas inasmuch as the derivative has the same value with respect to either a body or a stability system of axes to the second order in α.

CONCLUDING REMARKS

By means of the expressions developed in NACA Technical Note 2898, the span load distributions for families of thin sweptback wings sideslipping at an angle of attack have been calculated. Variations of the rolling-moment coefficient C_l with sideslip angle and of the corresponding stability derivative C_{l_β} with Mach number are also presented. The results are applicable to plan forms for which the wing tips are parallel to the wing axis of symmetry and, in general, at supersonic speeds for which the trailing edge is supersonic.

Langley Aeronautical Laboratory,
National Advisory Committee for Aeronautics,
Langley Field, Va., August 28, 1953.

REFERENCES

1. Hannah, Margery E., and Margolis, Kenneth: Span Load Distributions Resulting From Constant Angle of Attack, Steady Rolling Velocity, Steady Pitching Velocity, and Constant Vertical Acceleration for Tapered Sweptback Wings With Streamwise Tips - Subsonic Leading Edges and Supersonic Trailing Edges. NACA TN 2831, 1952.

2. Martin, John C., and Jeffreys, Isabella: Span Load Distributions Resulting From Angle of Attack, Rolling, and Pitching for Tapered Sweptback Wings With Streamwise Tips. Supersonic Leading and Trailing Edges. NACA TN 2643, 1952.

3. Margolis, Kenneth, Sherman, Windsor L., and Hannah, Margery E.: Theoretical Calculation of the Pressure Distribution, Span Loading, and Rolling Moment Due to Sideslip at Supersonic Speeds for Thin Sweptback Tapered Wings With Supersonic Trailing Edges and Wing Tips Parallel to the Axis of Wing Symmetry. NACA TN 2898, 1953.

4. Harmon, Sidney M., and Jeffreys, Isabella: Theoretical Lift and Damping in Roll of Thin Wings With Arbitrary Sweep and Taper at Supersonic Speeds. Supersonic Leading and Trailing Edges. NACA TN 2114, 1950.

5. Malvestuto, Frank S., Jr., Margolis, Kenneth, and Ribner, Herbert S.: Theoretical Lift and Damping in Roll at Supersonic Speeds of Thin Sweptback Tapered Wings With Streamwise Tips, Subsonic Leading Edges, and Supersonic Trailing Edges. NACA Rep. 970, 1950. (Supersedes NACA TN 1860.)

6. Jones, Arthur L., Spreiter, John R., and Alksne, Alberta: The Rolling Moment Due to Sideslip of Triangular, Trapezoidal, and Related Plan Forms in Supersonic Flow. NACA TN 1700, 1948.

TABLE I

INDEX TO CHARTS FOR SPAN LOAD DISTRIBUTIONS

Λ, deg	A	λ	Mach number range	Figure
30	2.0	0.50	1.4 to 3.2	3
	4.0	.25	1.1	4(a)
	4.0	.50	1.1 to 3.2	4(b) to (g)
45	2.0	.50	1.1 to 3.2	5
	4.0	.25	1.2	6(a)
	4.0	.50	1.4 to 3.2	6(b) to (f)
60	2.0	.25	1.2 to 1.6	7(a) to (c)
	2.0	.50	2.0 to 3.2	7(d) to (g)
	4.0	.50	2.0 to 3.2	8

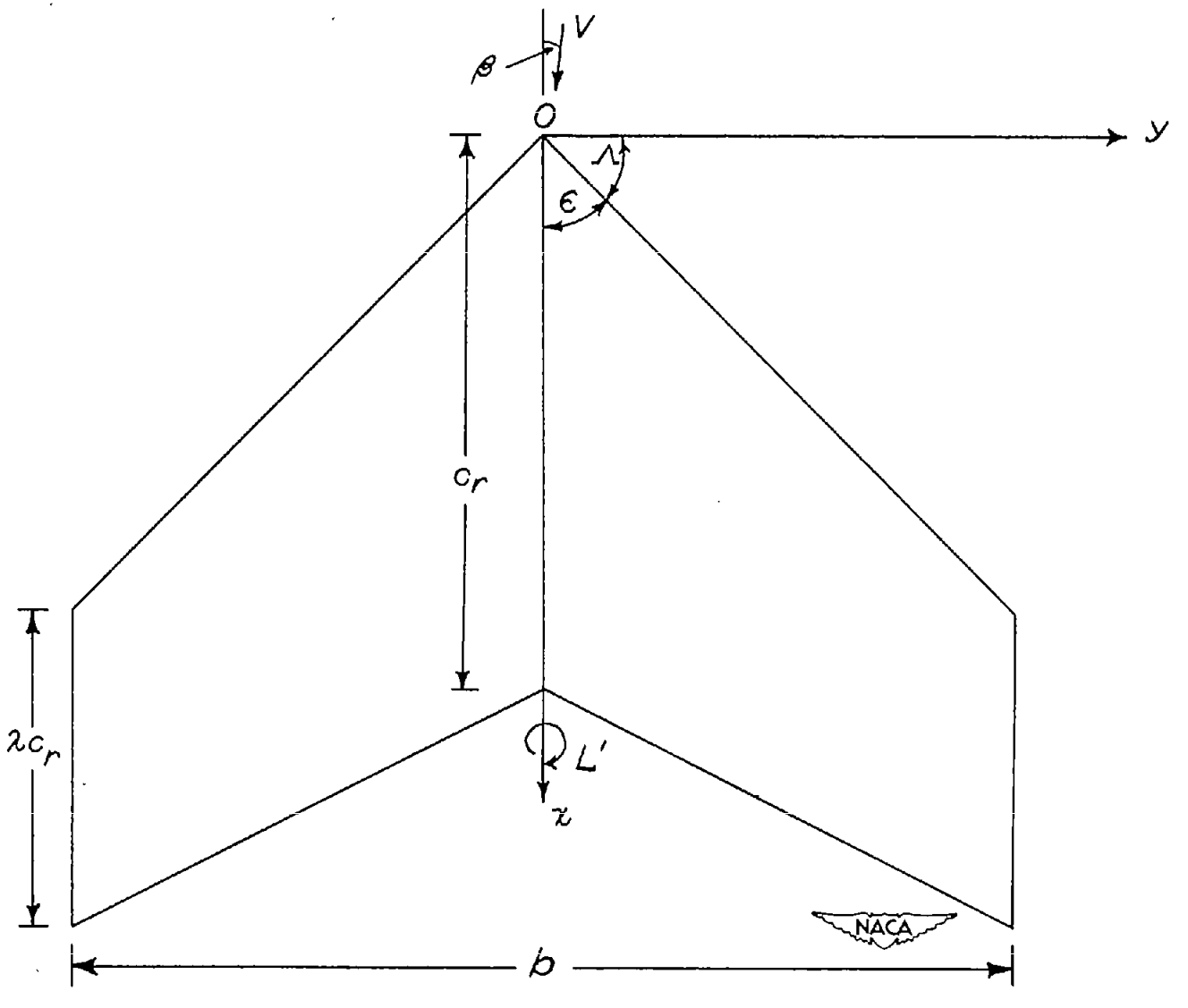

Figure 1.- Symbols and pertinent data associated with general wing plan form.

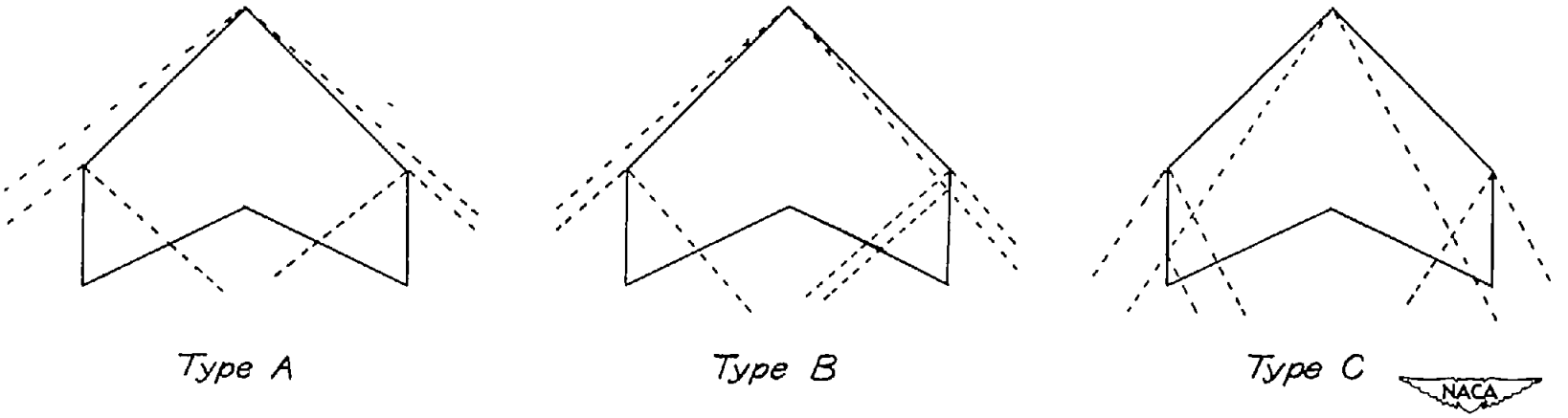

Figure 2.- Types of plan-form—Mach line configurations.

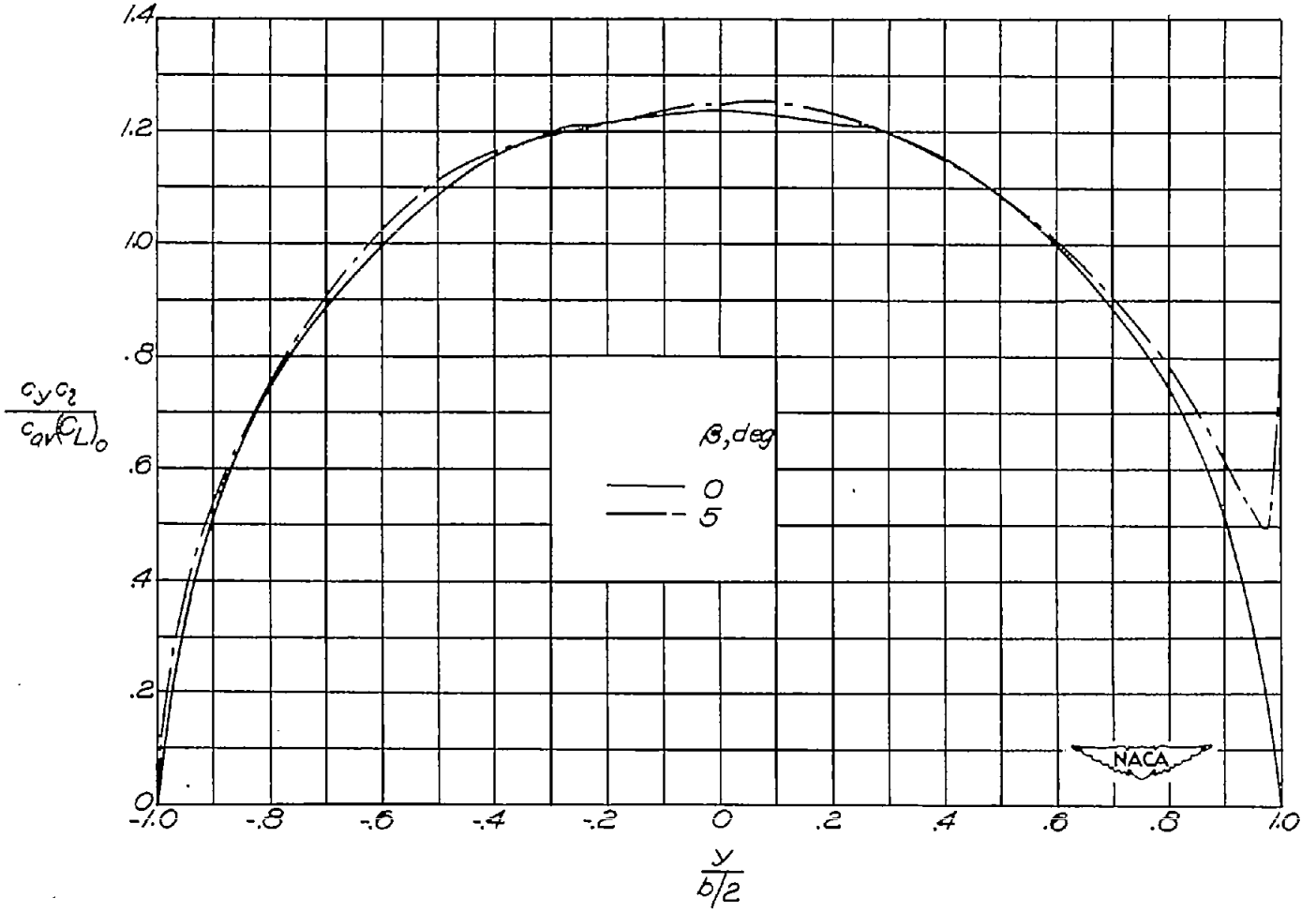

(a) M = 1.4.

Figure 3.- Span loadings for various sideslip angles. $\Lambda = 30^{\circ}$; $\lambda = 0.50$; $A = 2.0$.

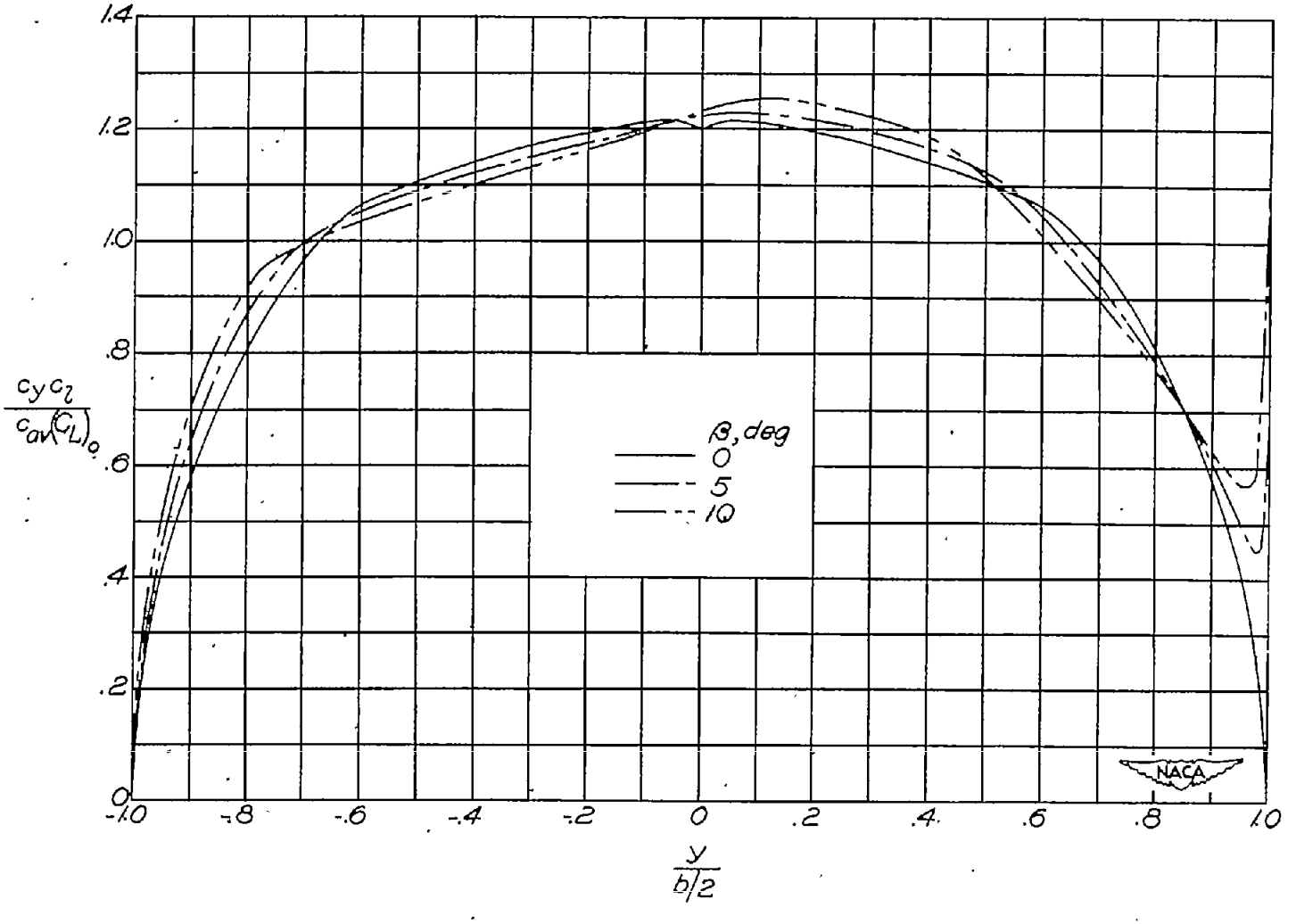

(b) M = 2.0.

Figure 3.- Continued.

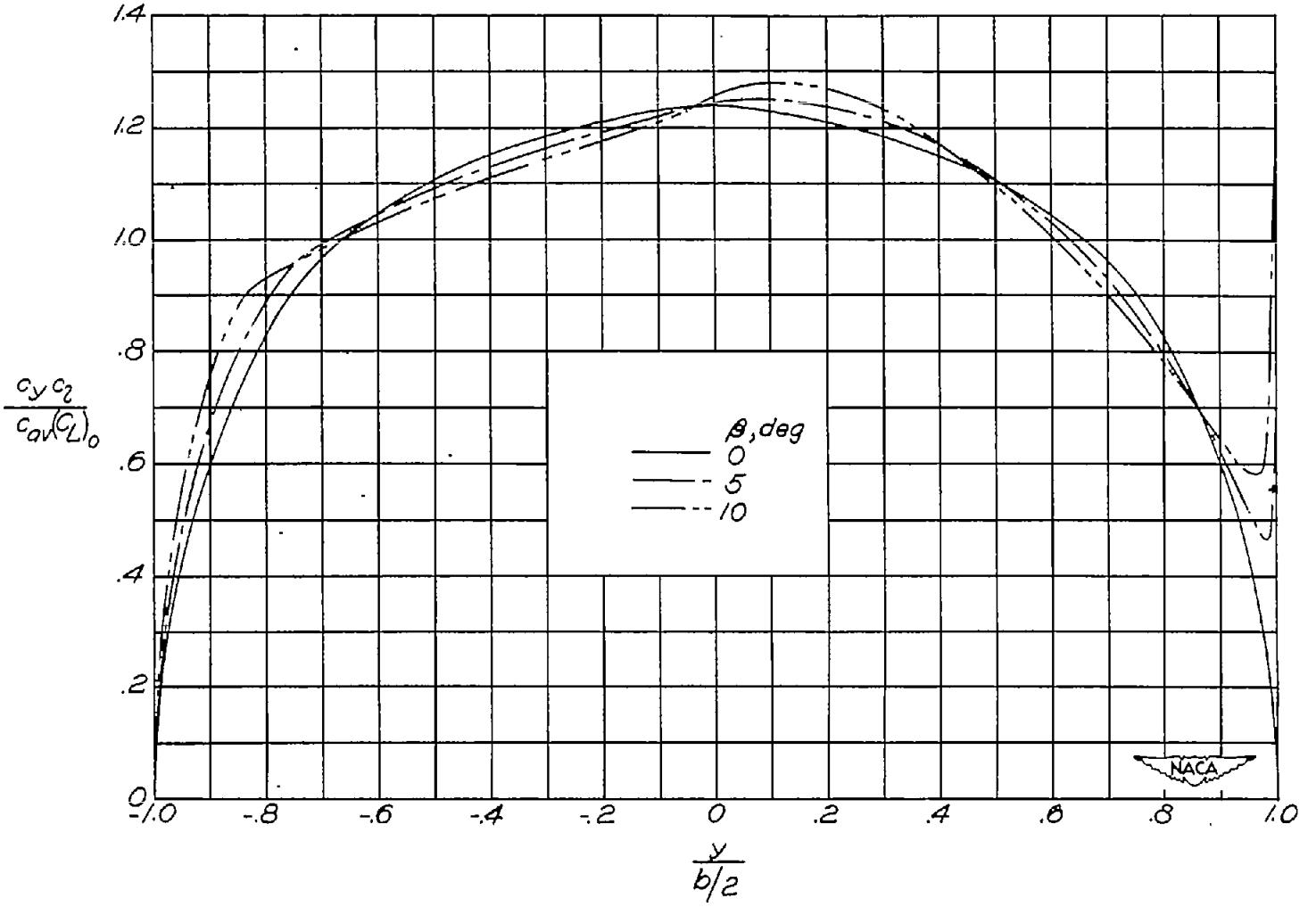

(c) M = 2.4.

Figure 3.- Continued.

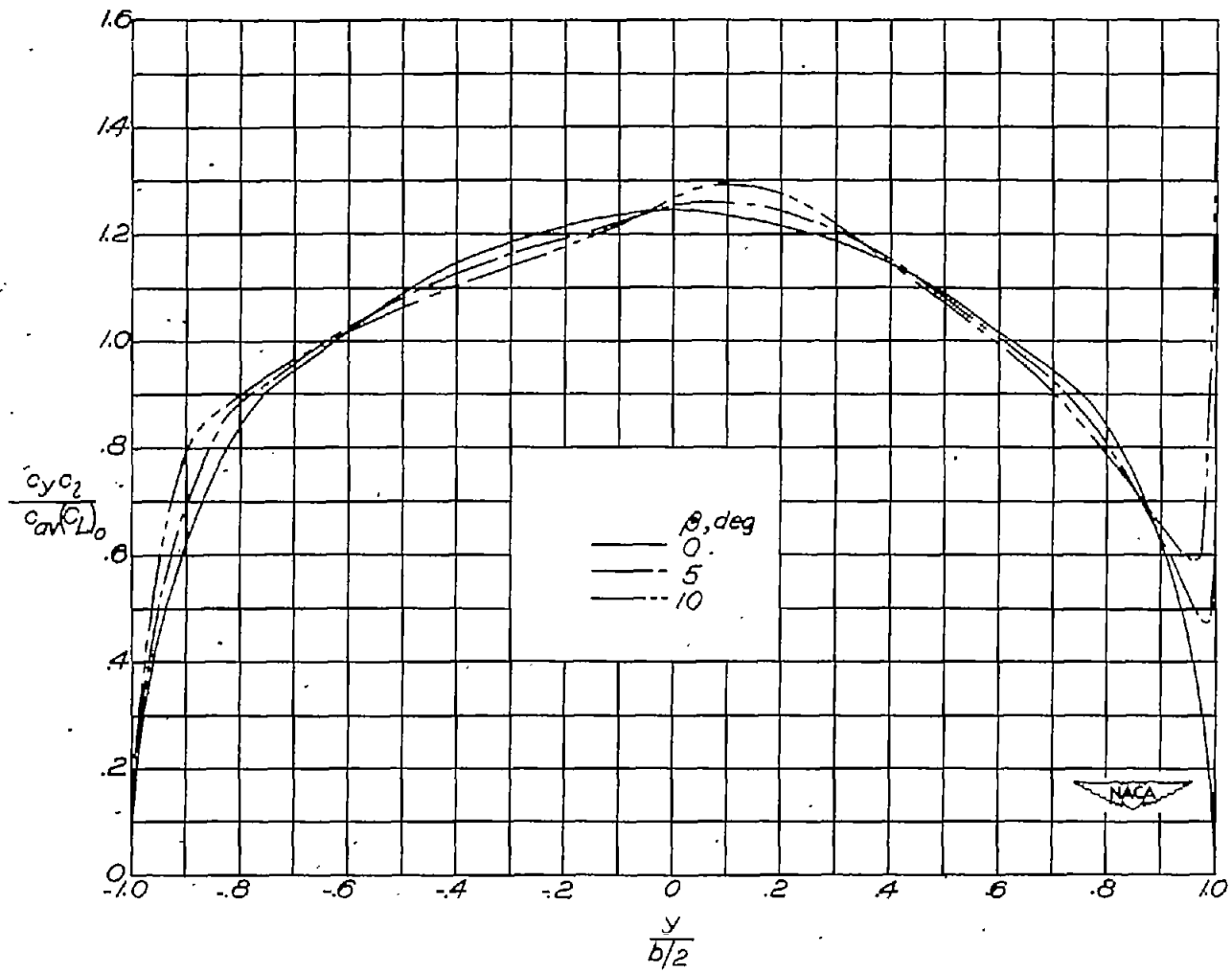

(d) M = 2.8.

Figure 3.- Continued.

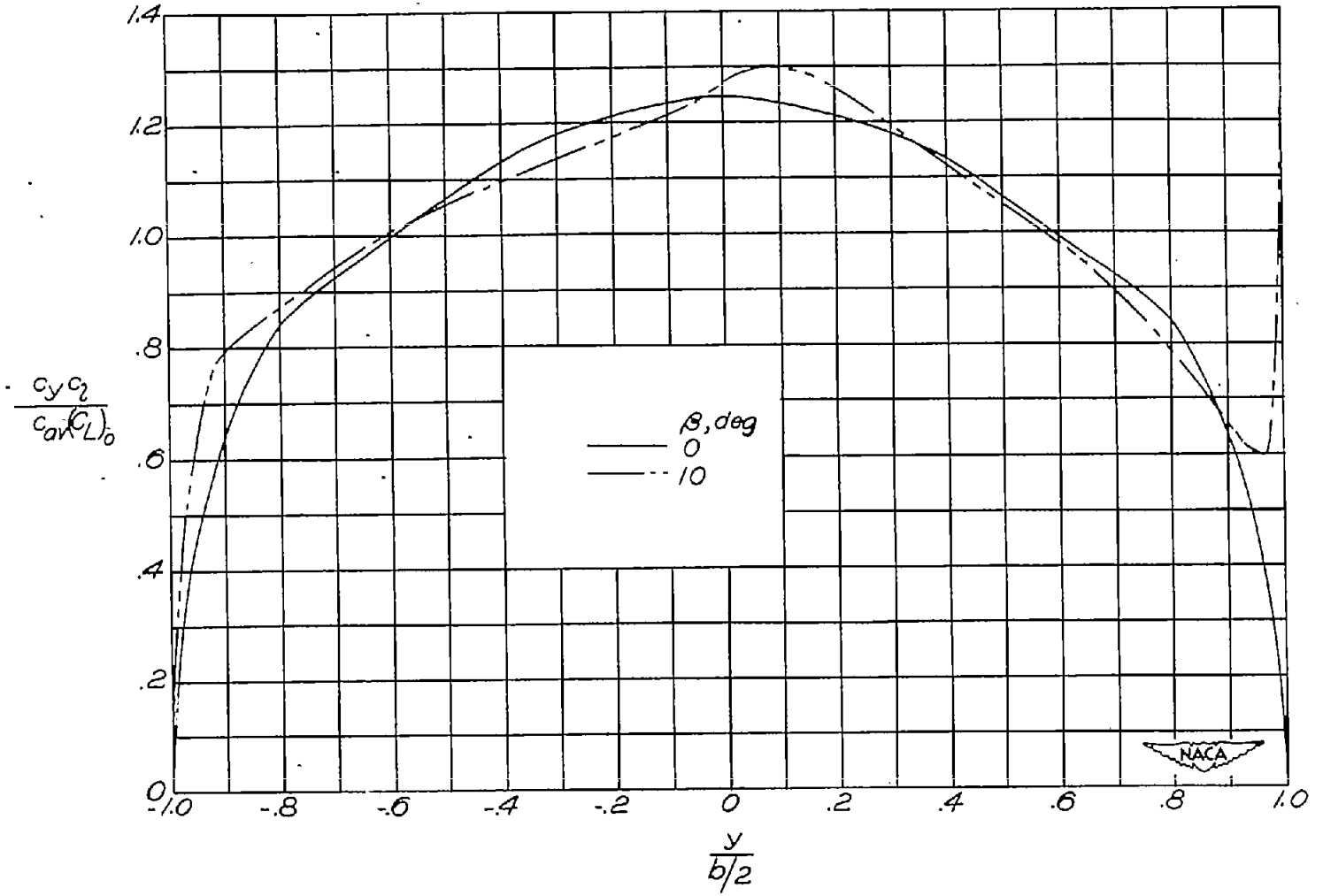

(e) M = 3.2.

Figure 3.- Concluded.

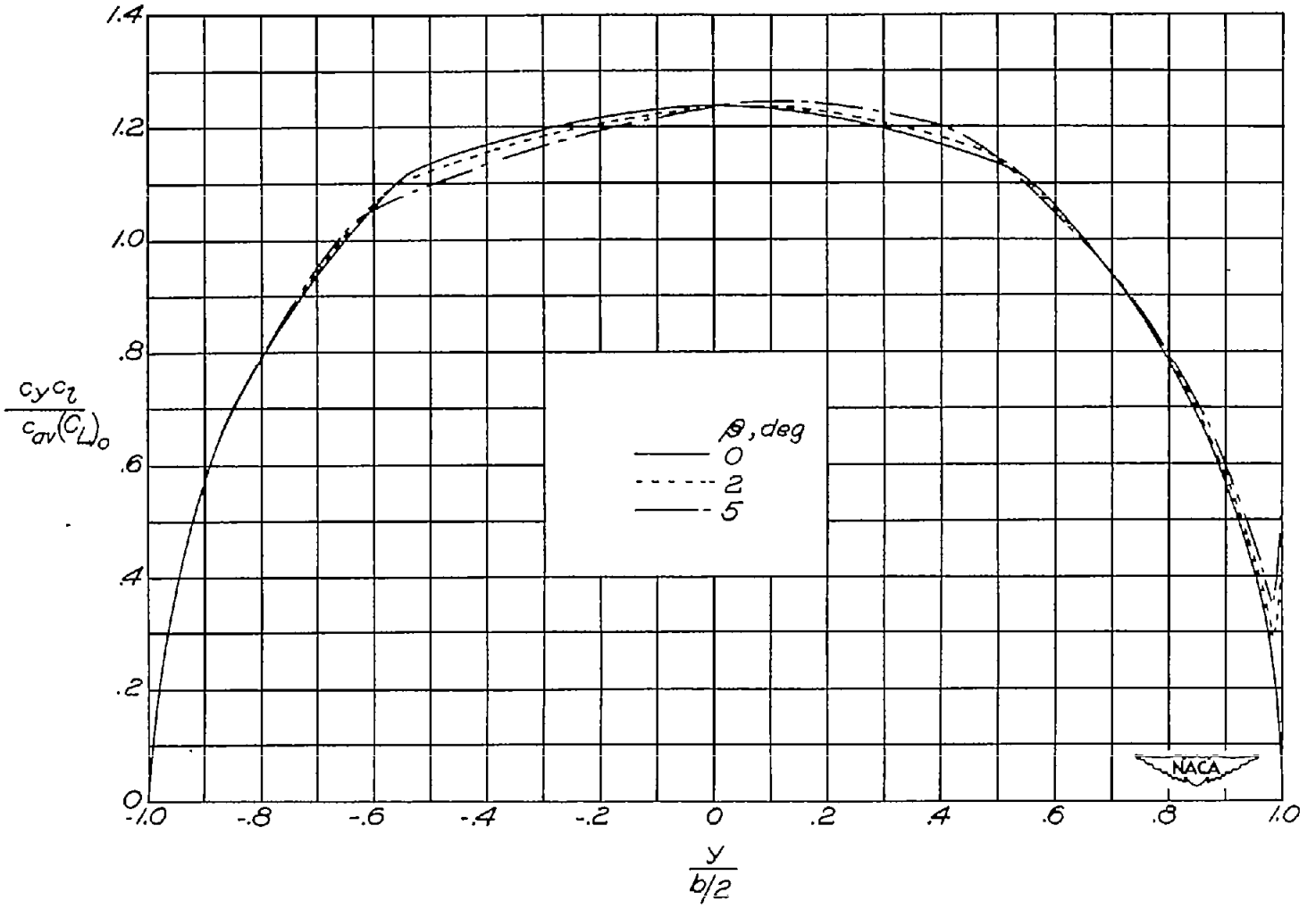

(a) $\lambda = 0.25$; $M = 1.1$.

Figure 4.- Span loadings for various sideslip angles. $\Lambda = 30^\circ$; $A = 4.0$.

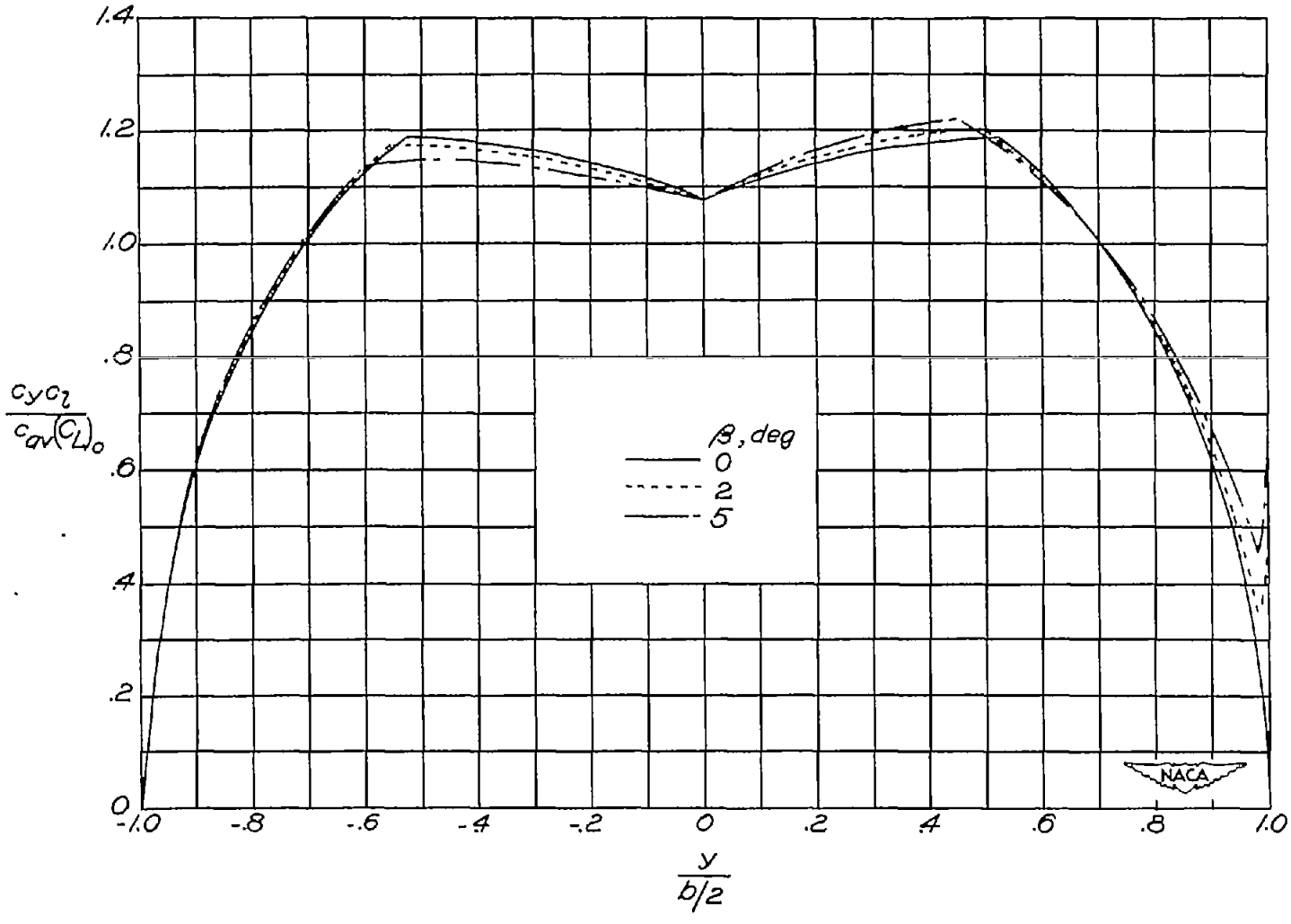

(b) $\lambda = 0.50$; $M = 1.1$.

Figure 4.- Continued.

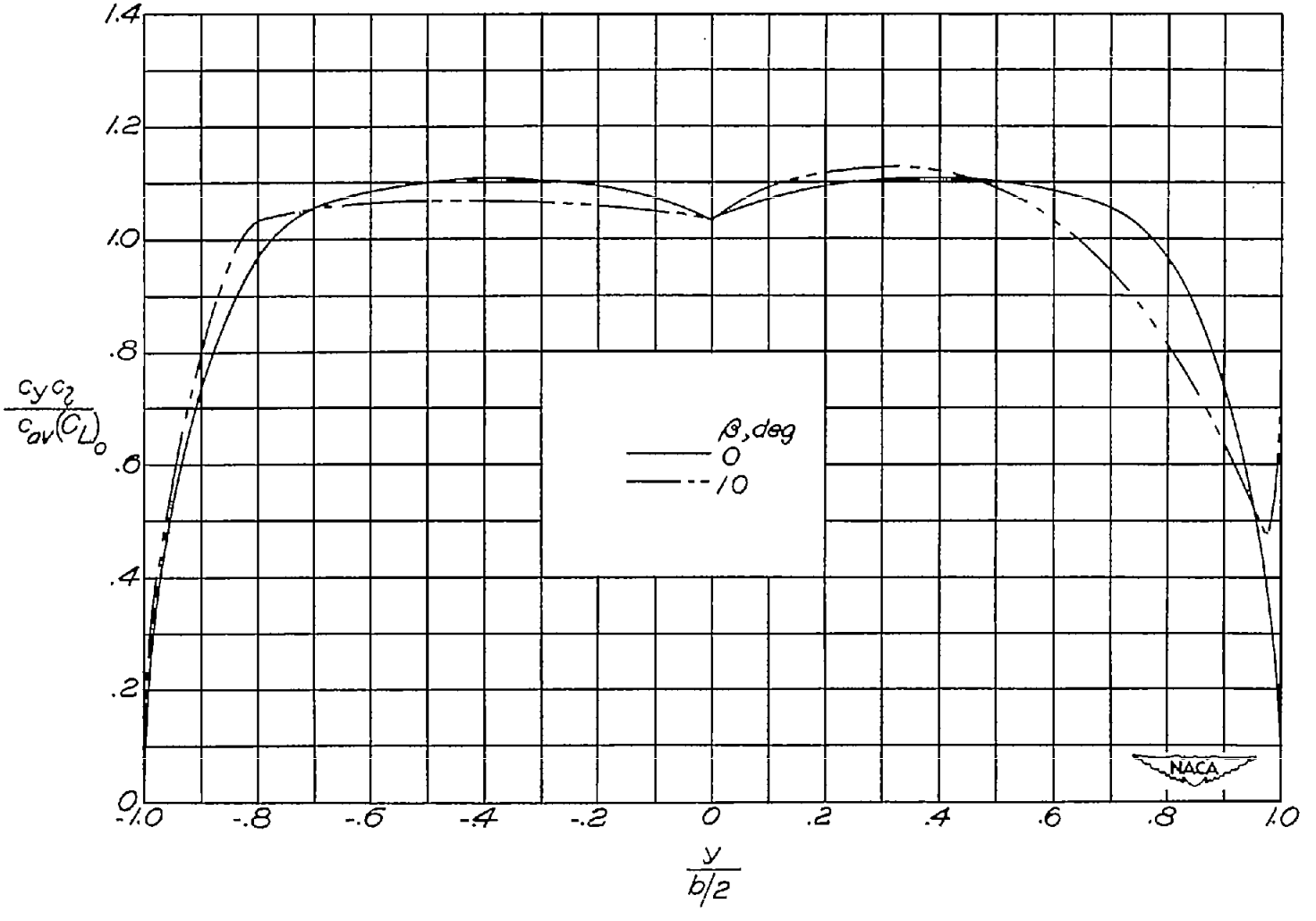

(c) $\lambda = 0.50$; $M = 1.4$.

Figure 4.- Continued.

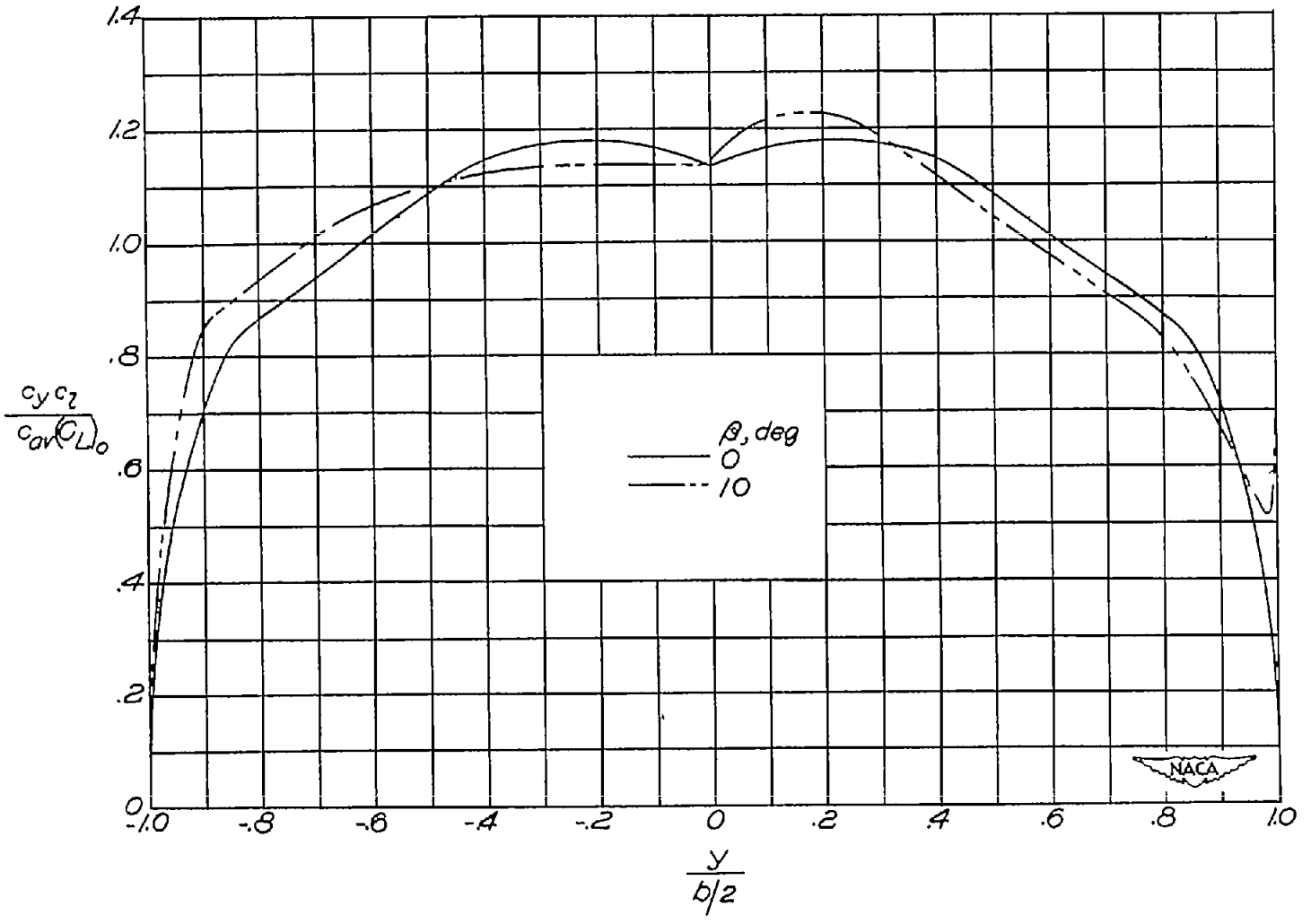

(d) $\lambda = 0.50$; $M = 2.0$.

Figure 4.- Continued.

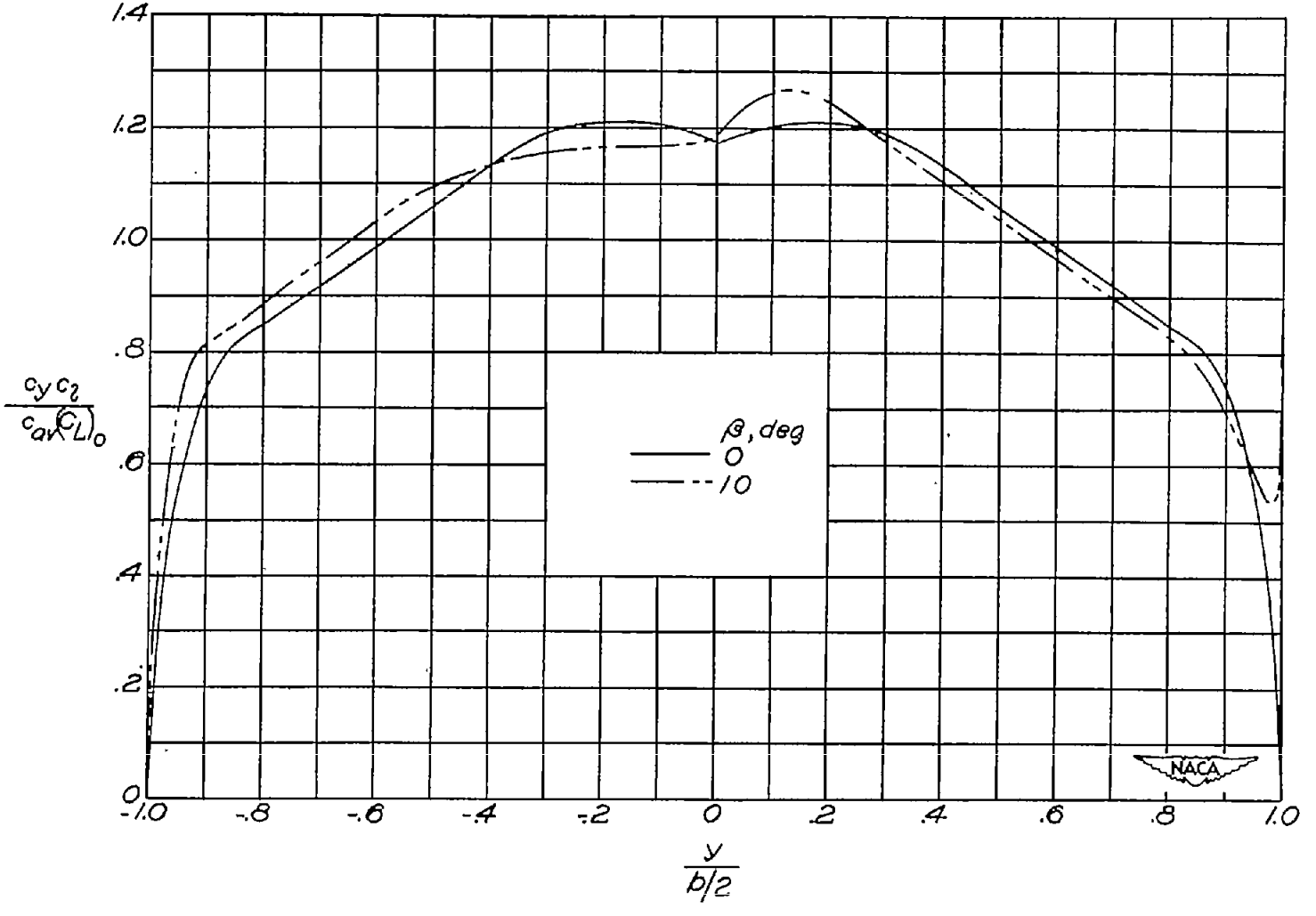

(e) $\lambda = 0.50$; $M = 2.4$.

Figure 4.- Continued.

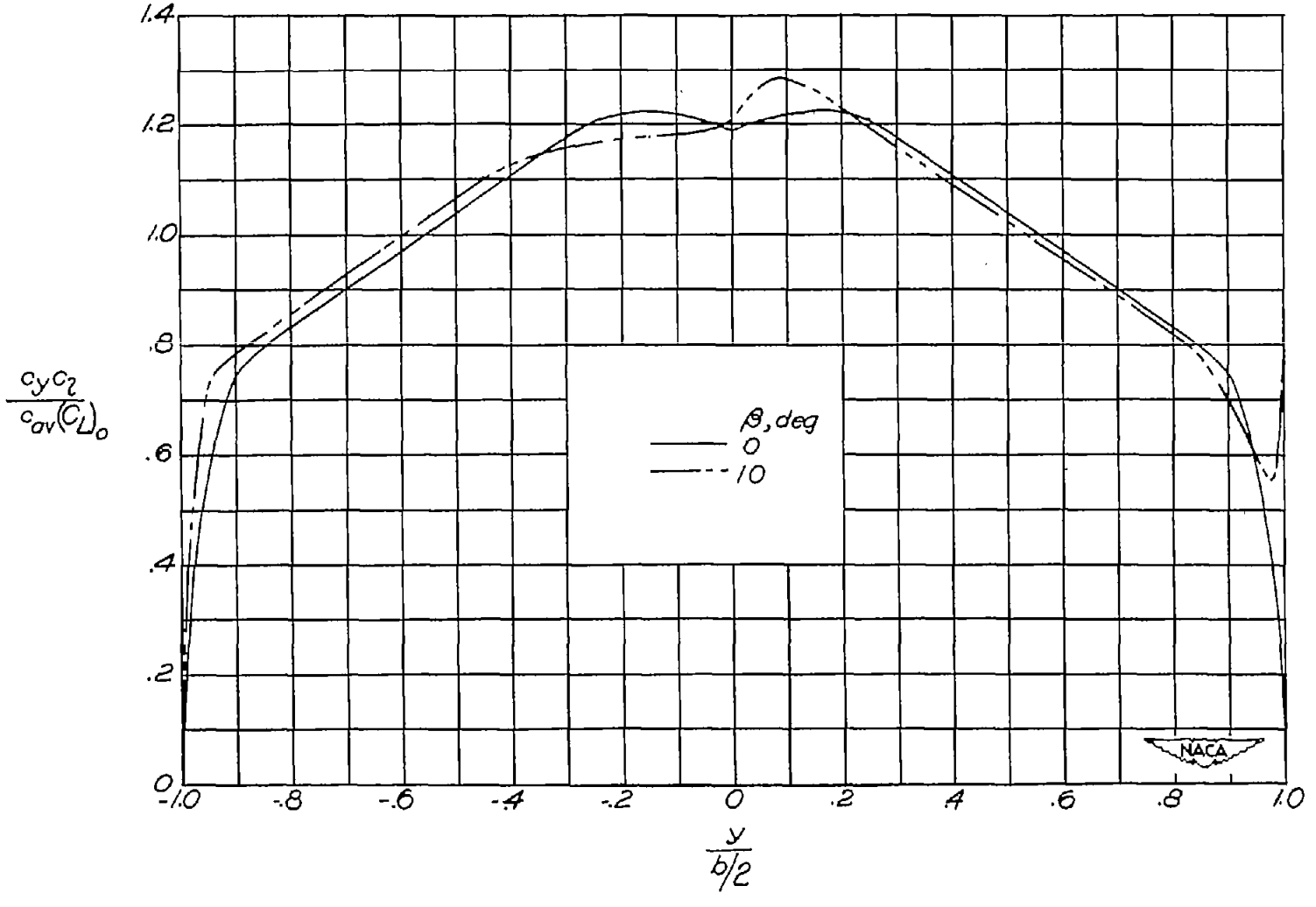

(f) $\lambda = 0.50$; $M = 2.8$.

Figure 4.- Continued.

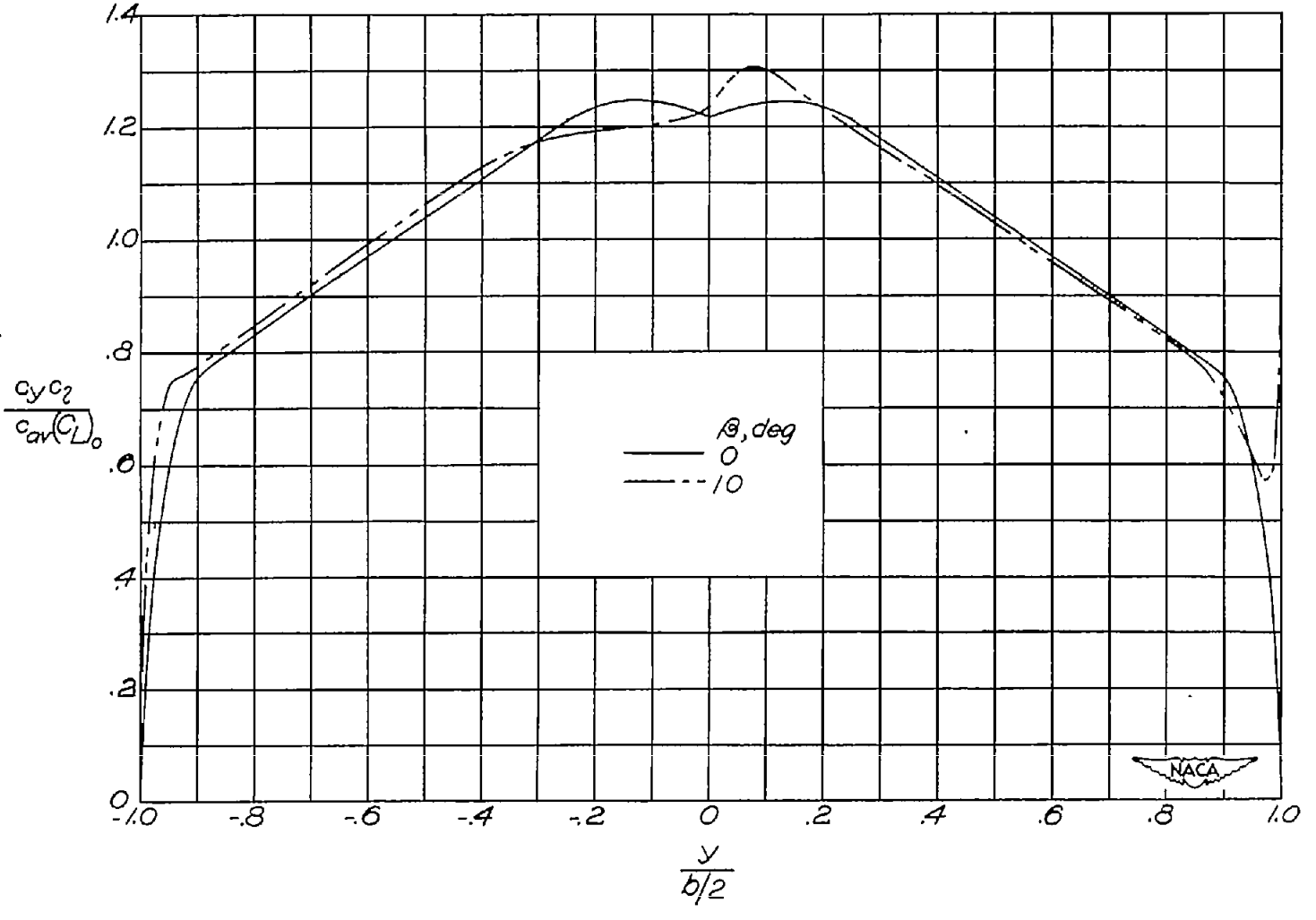

(g) $\lambda = 0.50$; $M = 3.2$.

Figure 4.- Concluded.

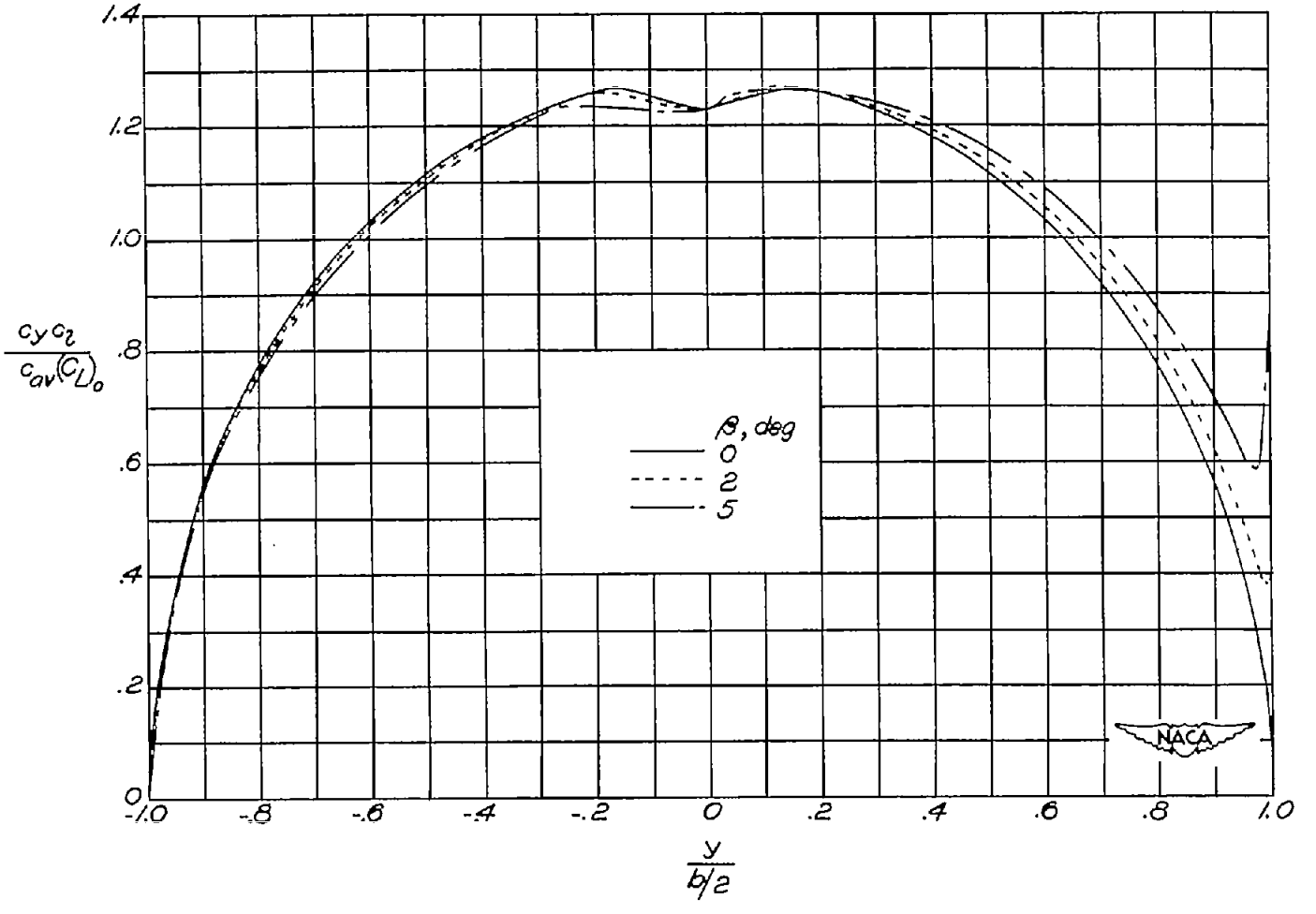

(a) M = 1.1.

Figure 5.- Span loadings for various sideslip angles. $\Lambda = 45^\circ$; $\lambda = 0.5$; $A = 2.0$.

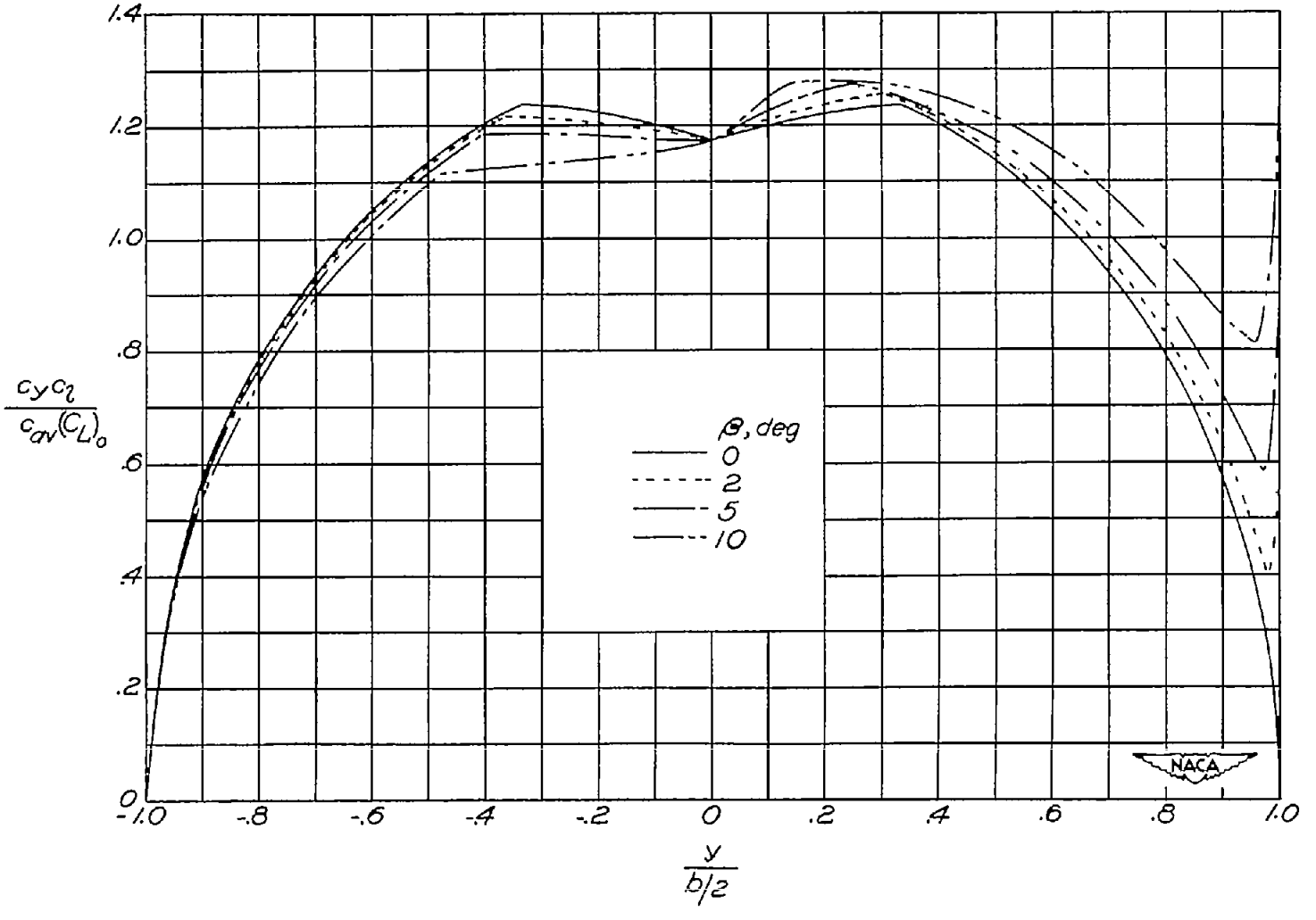

(b) M = 1.2.

Figure 5.- Continued.

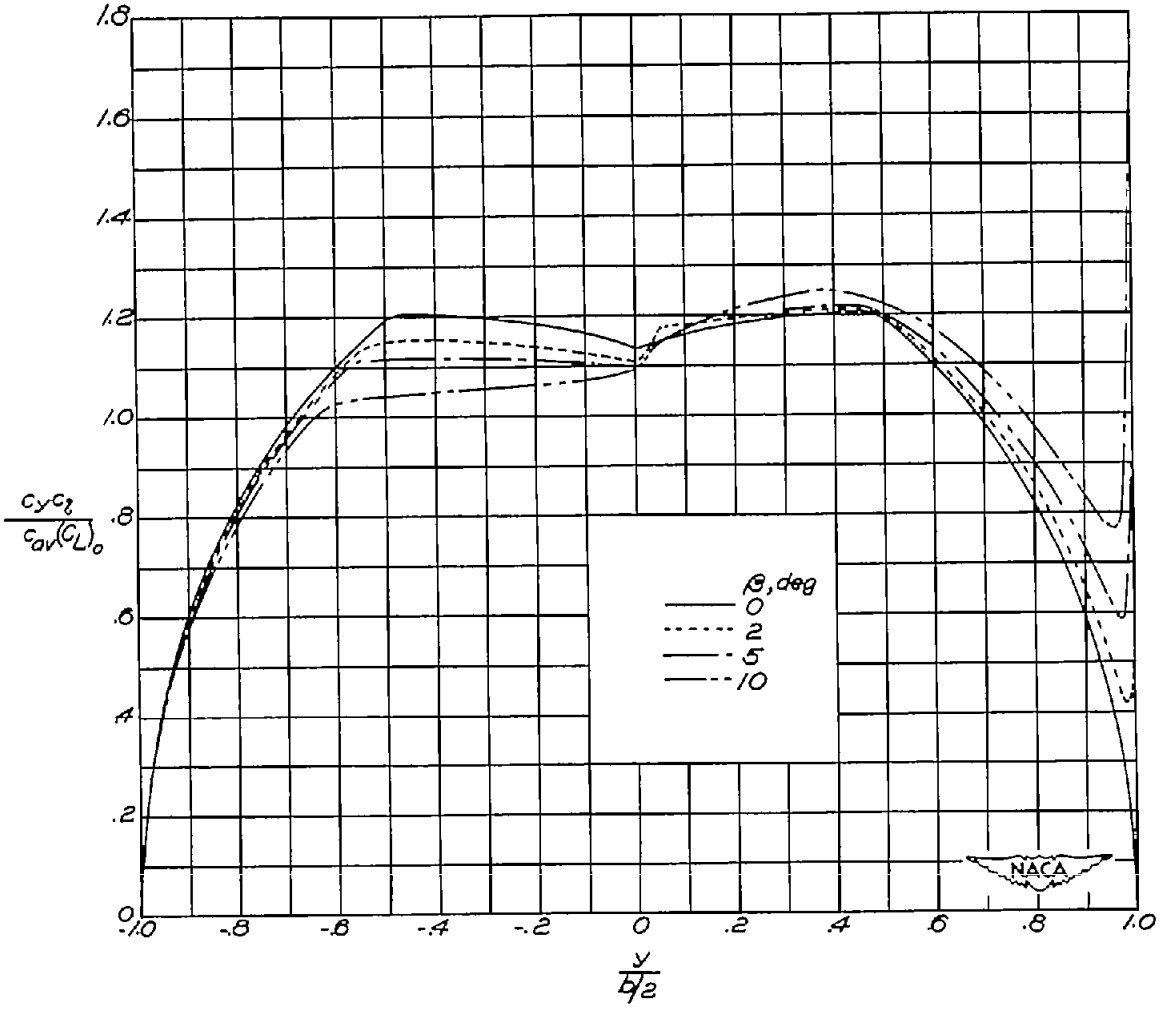

(c) M = 1.4.

Figure 5.- Continued.

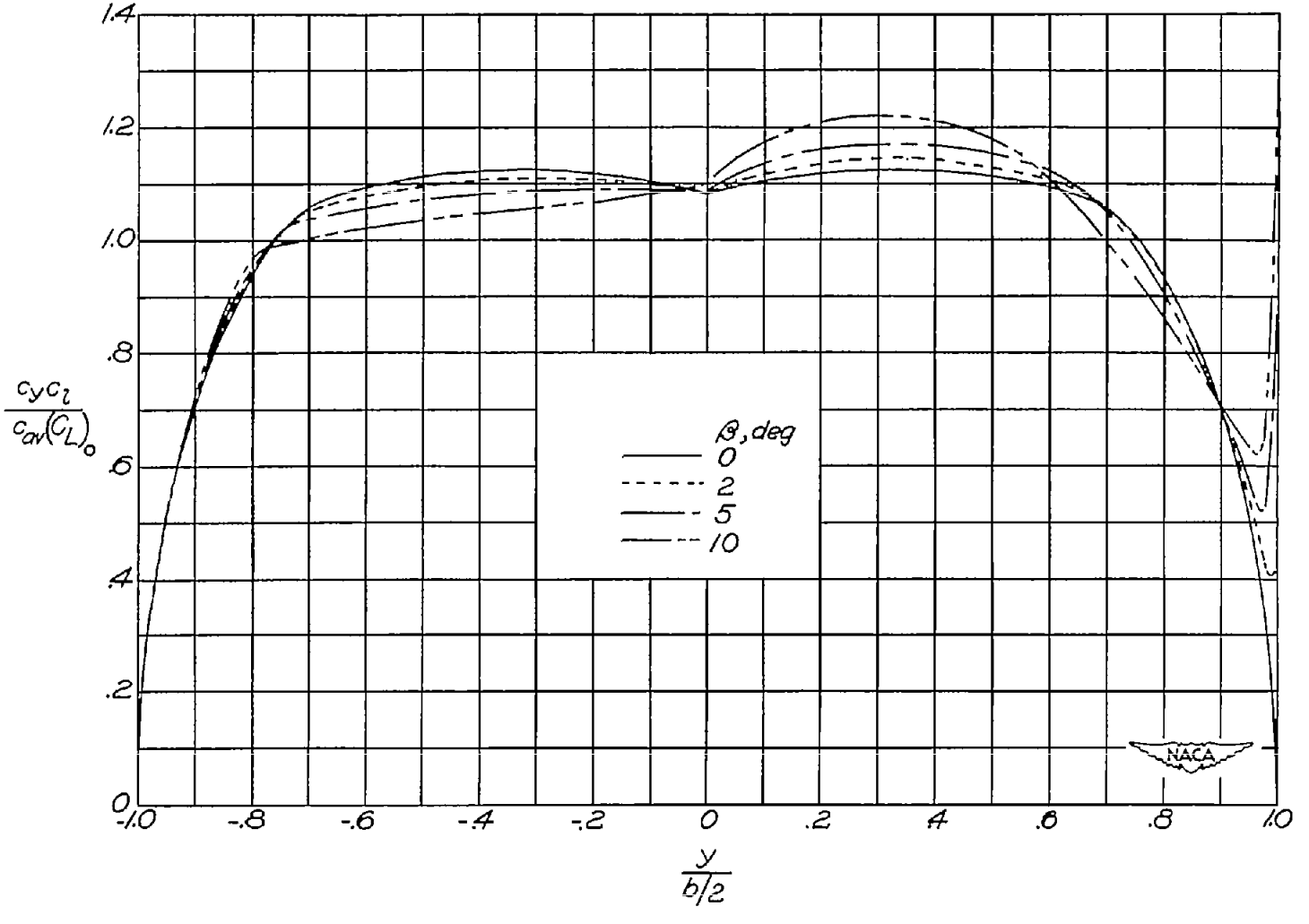

(d) M = 2.0.

Figure 5.- Continued.

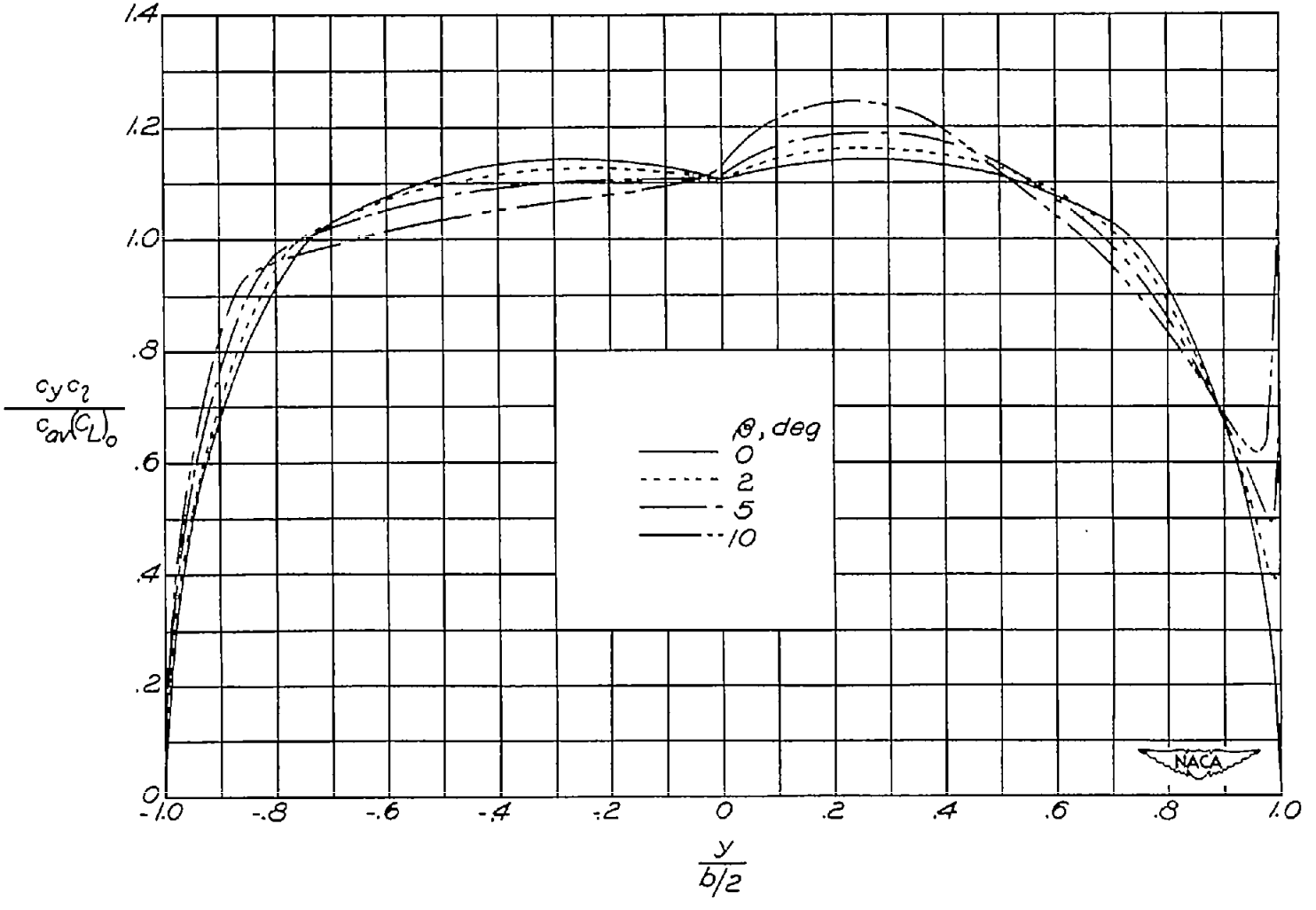

(e) M = 2.4.

Figure 5.- Continued.

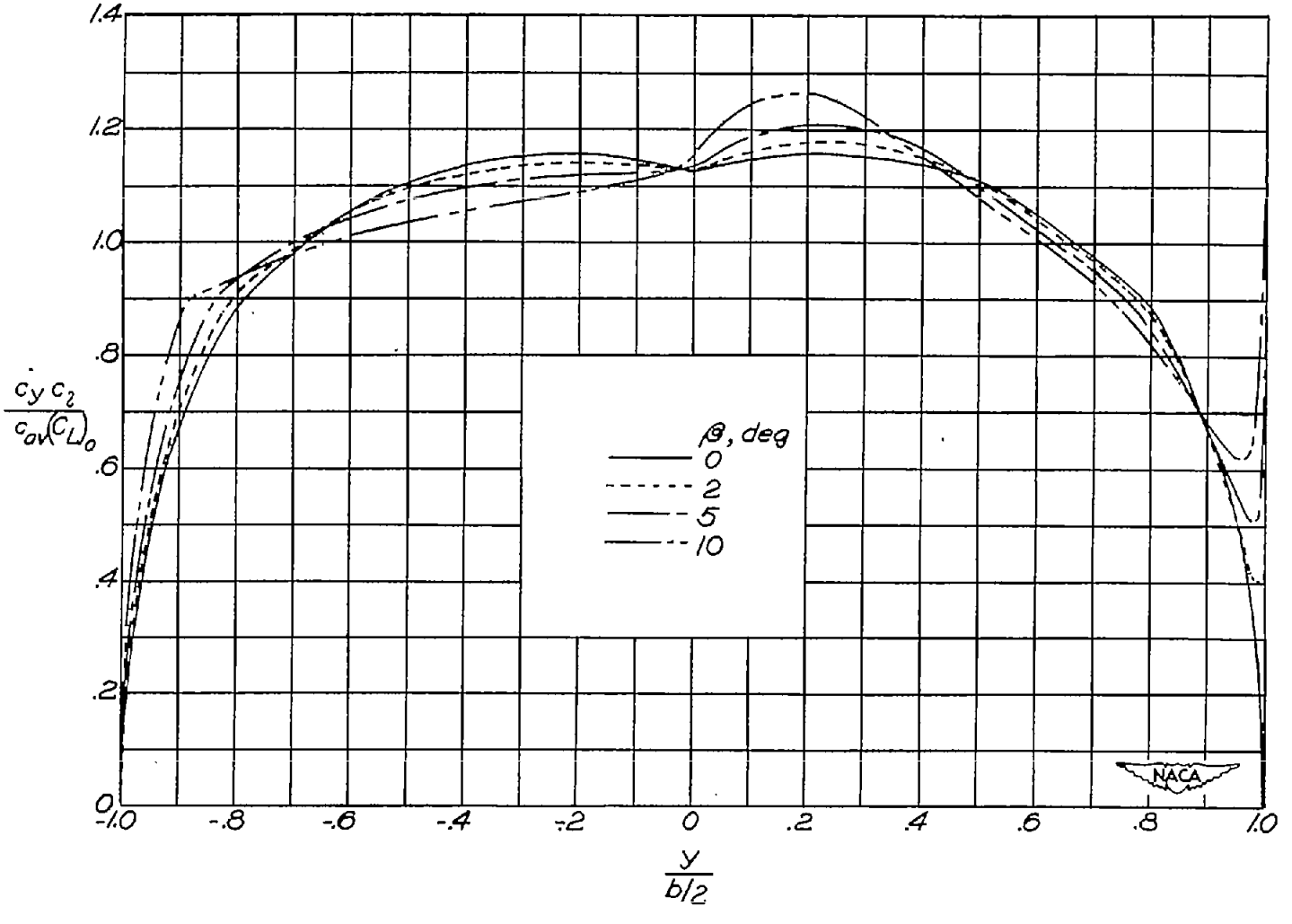

(f) M = 2.8.

Figure 5.- Continued.

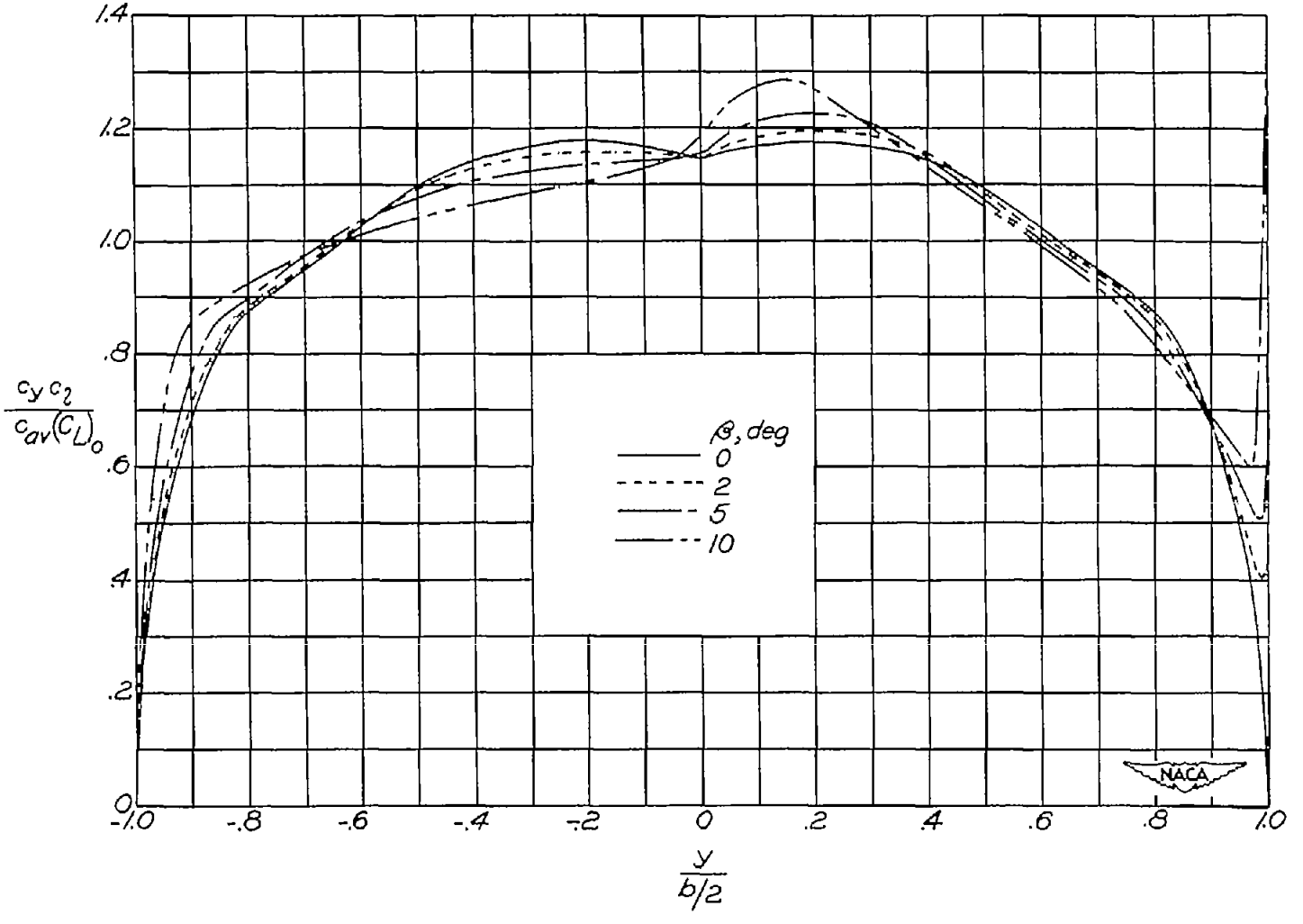

(g) M = 3.2.

Figure 5.- Concluded.

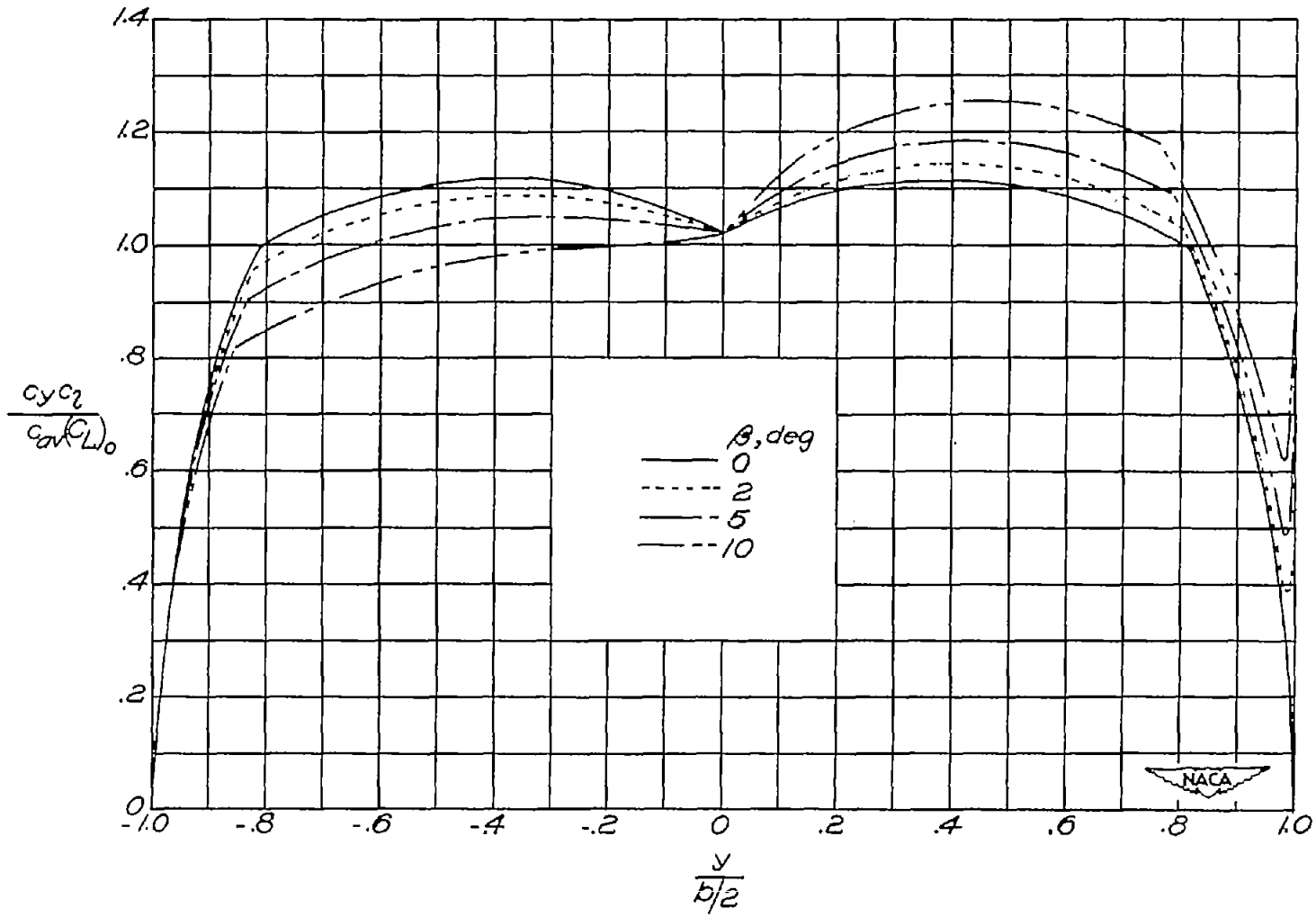

(a) $\lambda = 0.25$; $M = 1.2$.

Figure 6.- Span loadings for various sideslip angles. $\Lambda = 45^\circ$; $A = 4.0$.

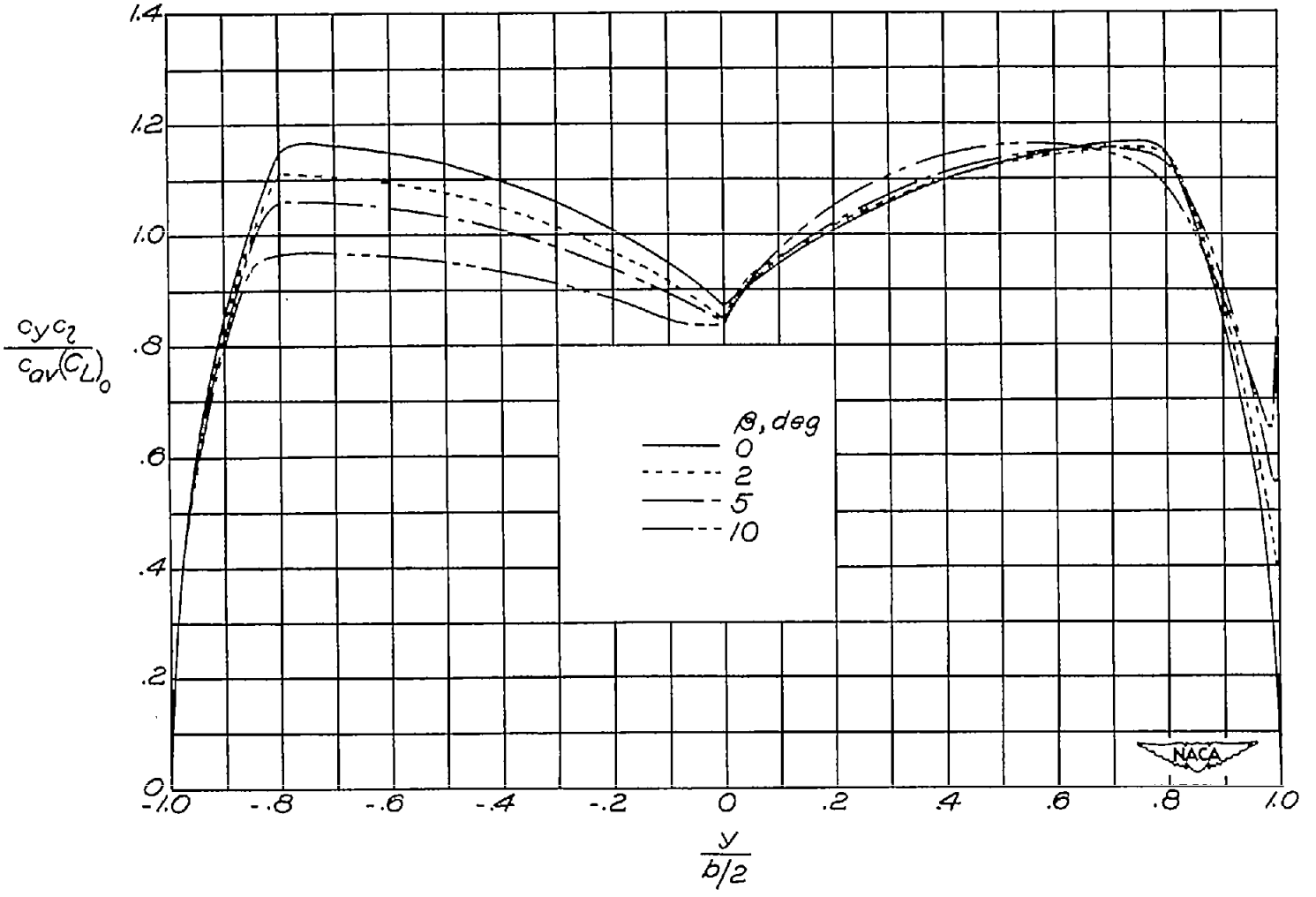

(b) $\lambda = 0.50$; $M = 1.4$.

Figure 6.- Continued.

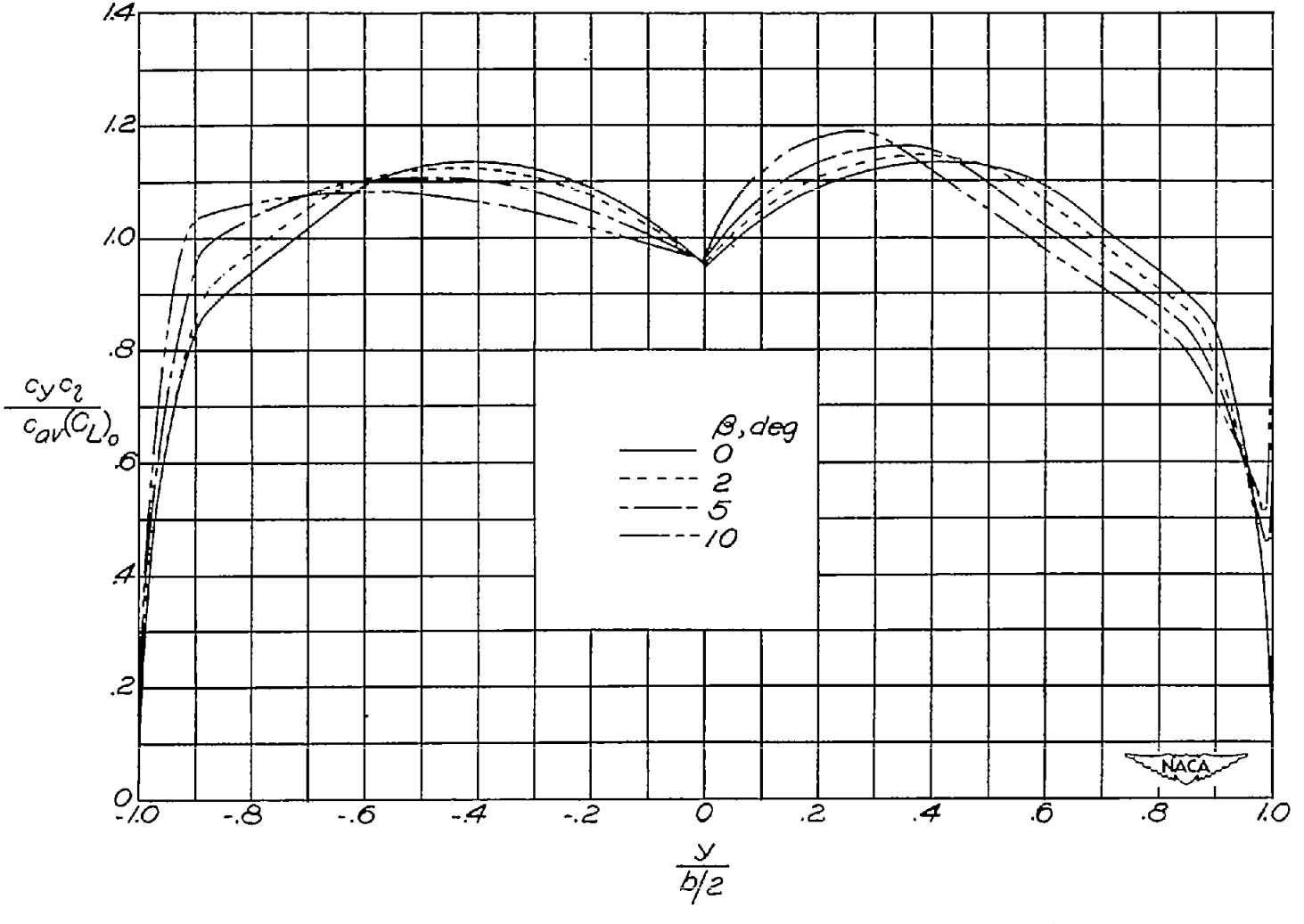

(c) $\lambda = 0.50$; $M = 2.0$.

Figure 6.- Continued.

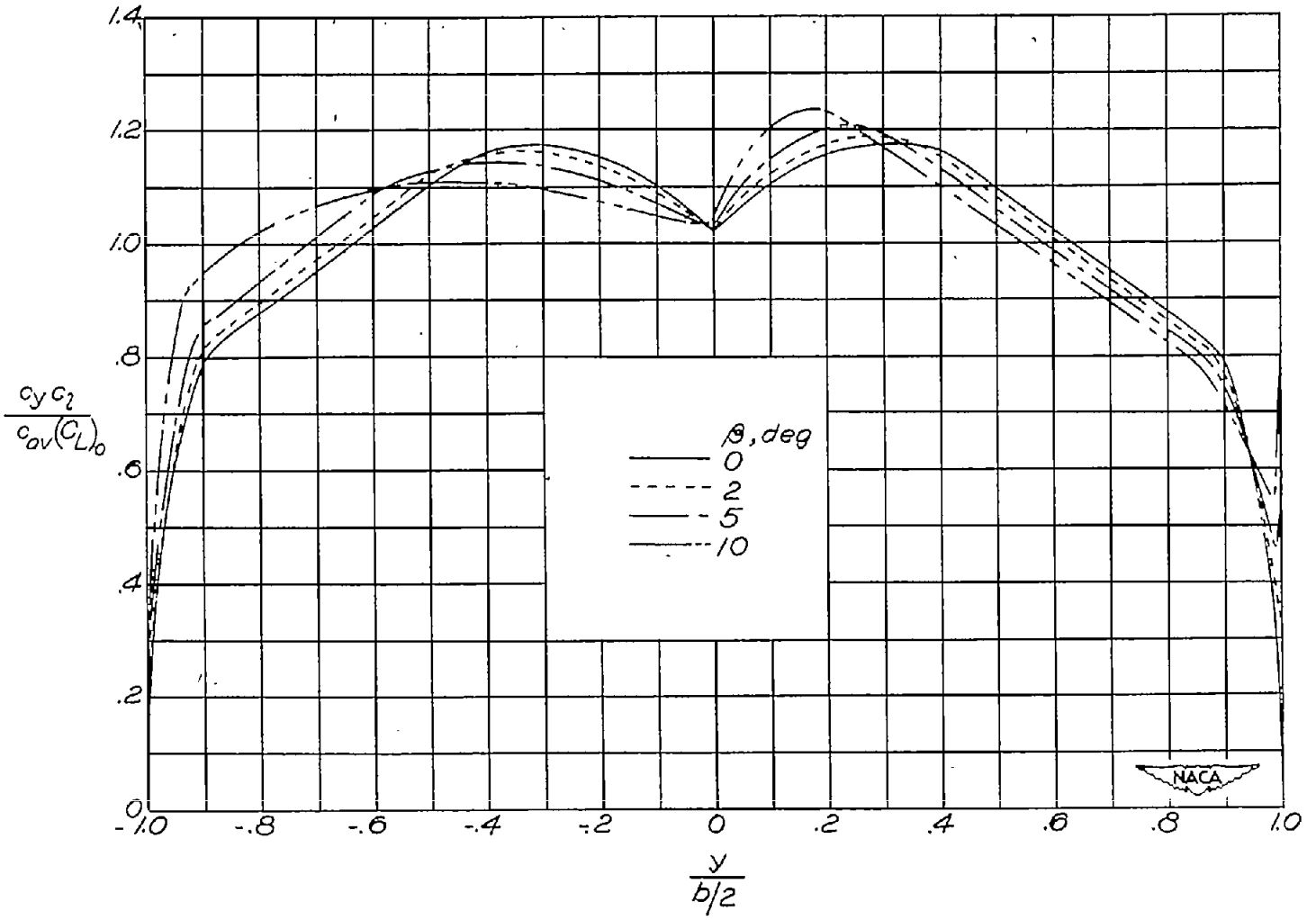

(d) $\lambda = 0.50$; $M = 2.4$.

Figure 6.- Continued.

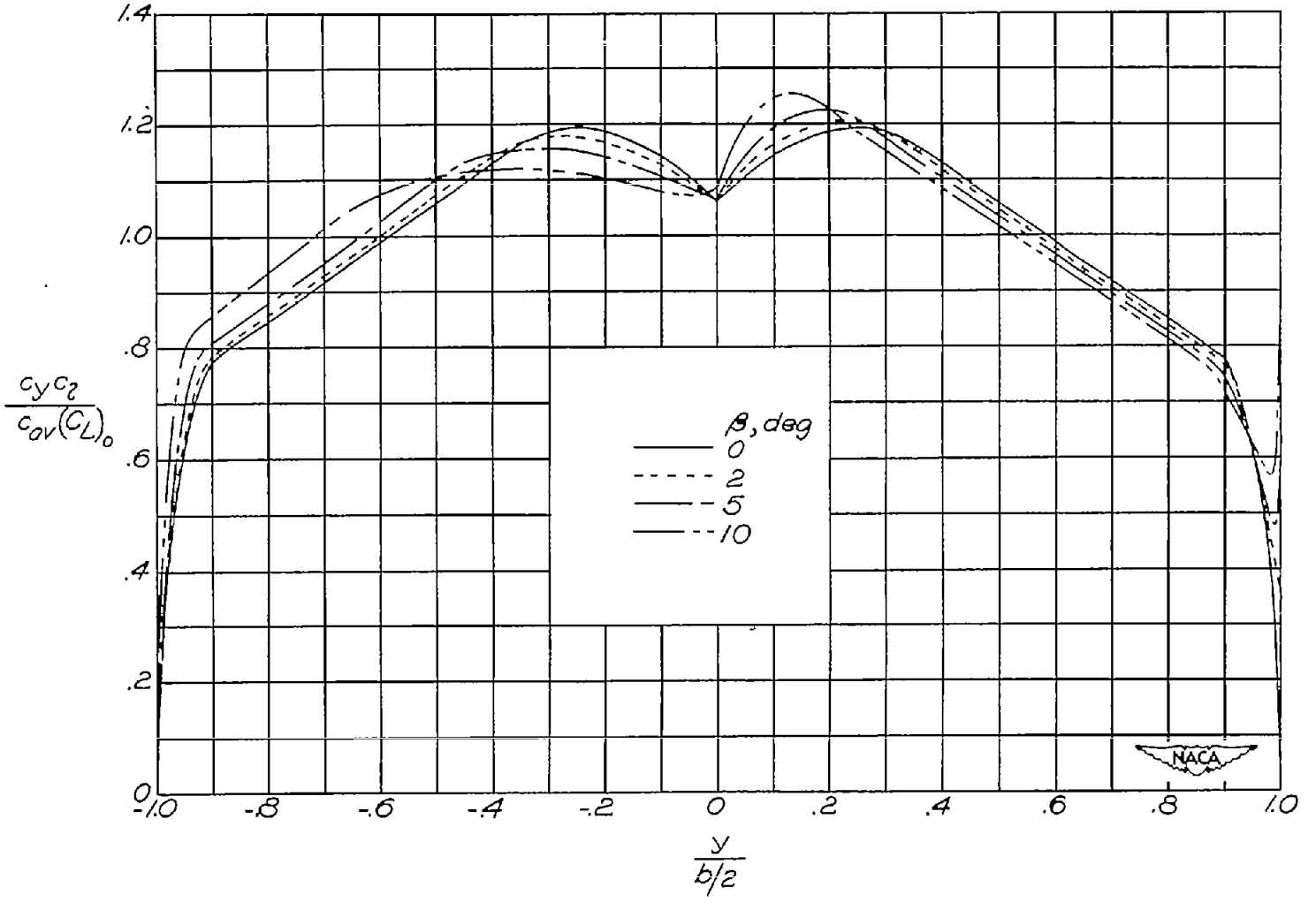

(e) $\lambda = 0.50$; $M = 2.8$.

Figure 6.- Continued.

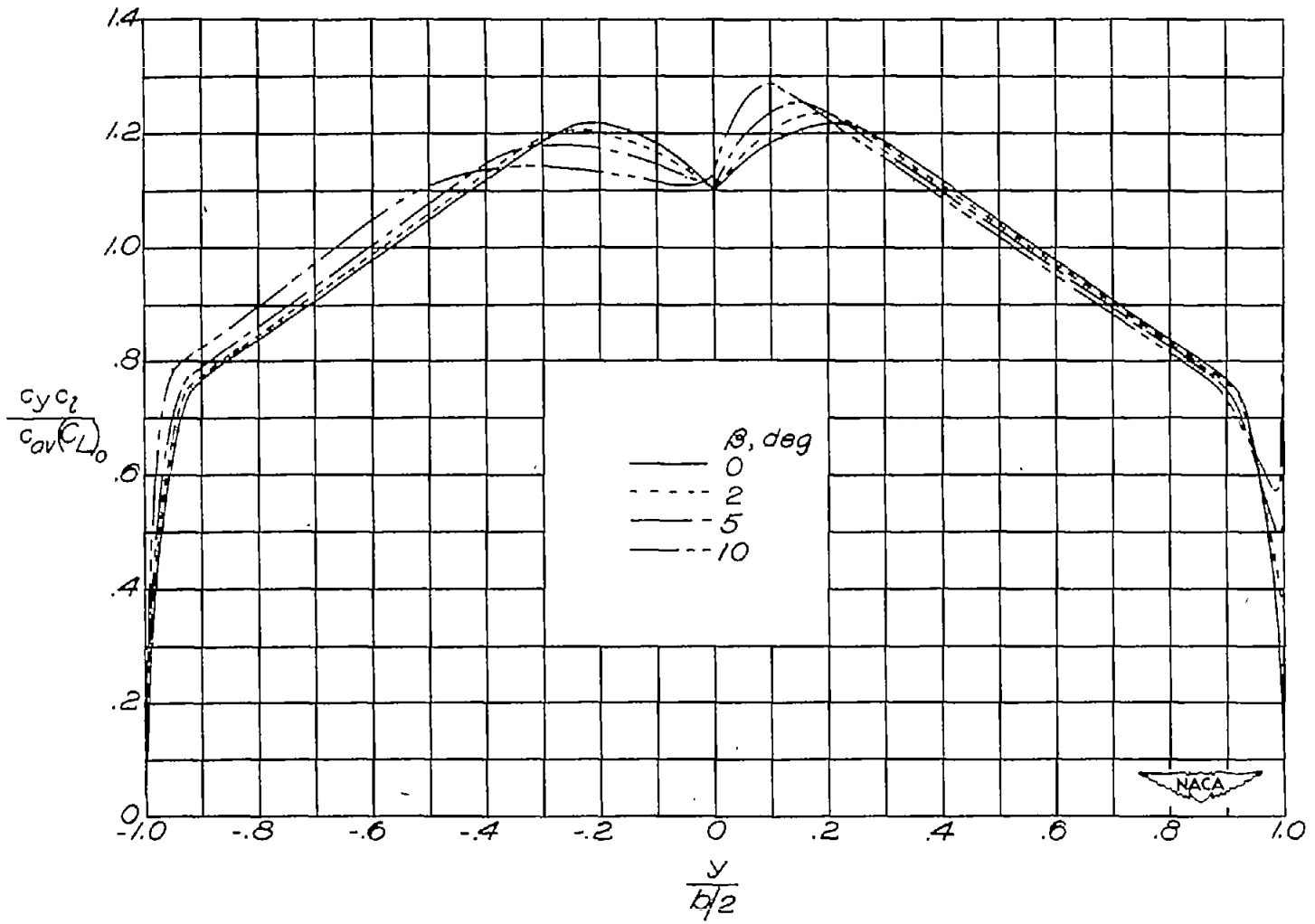

(f) $\lambda = 0.50$; $M = 3.2$.

Figure 6.- Concluded.

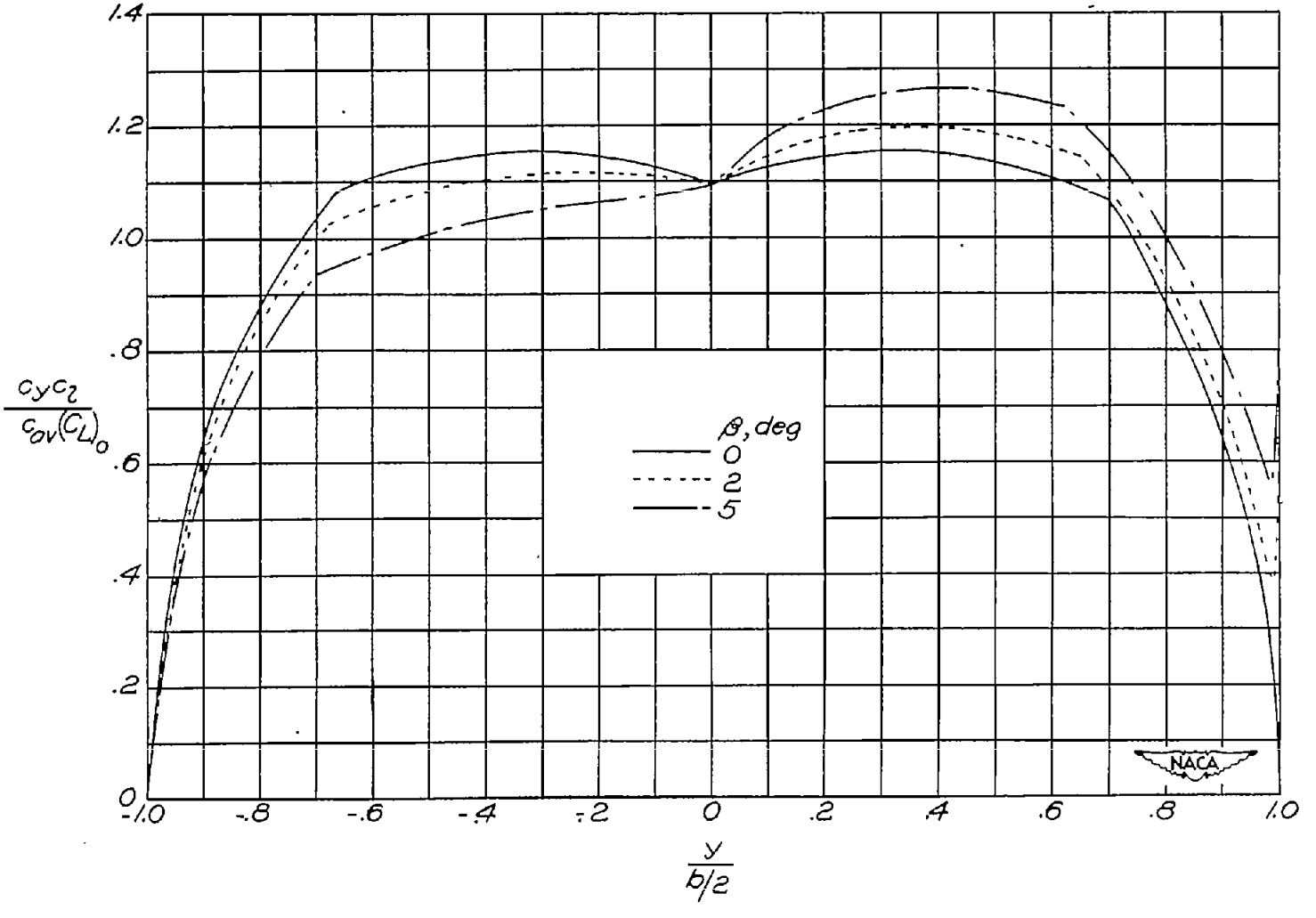

(a) $\lambda = 0.25$; $M = 1.2$.

Figure 7.- Span loadings for various sideslip angles. $\Lambda = 60^\circ$; $A = 2.0$.

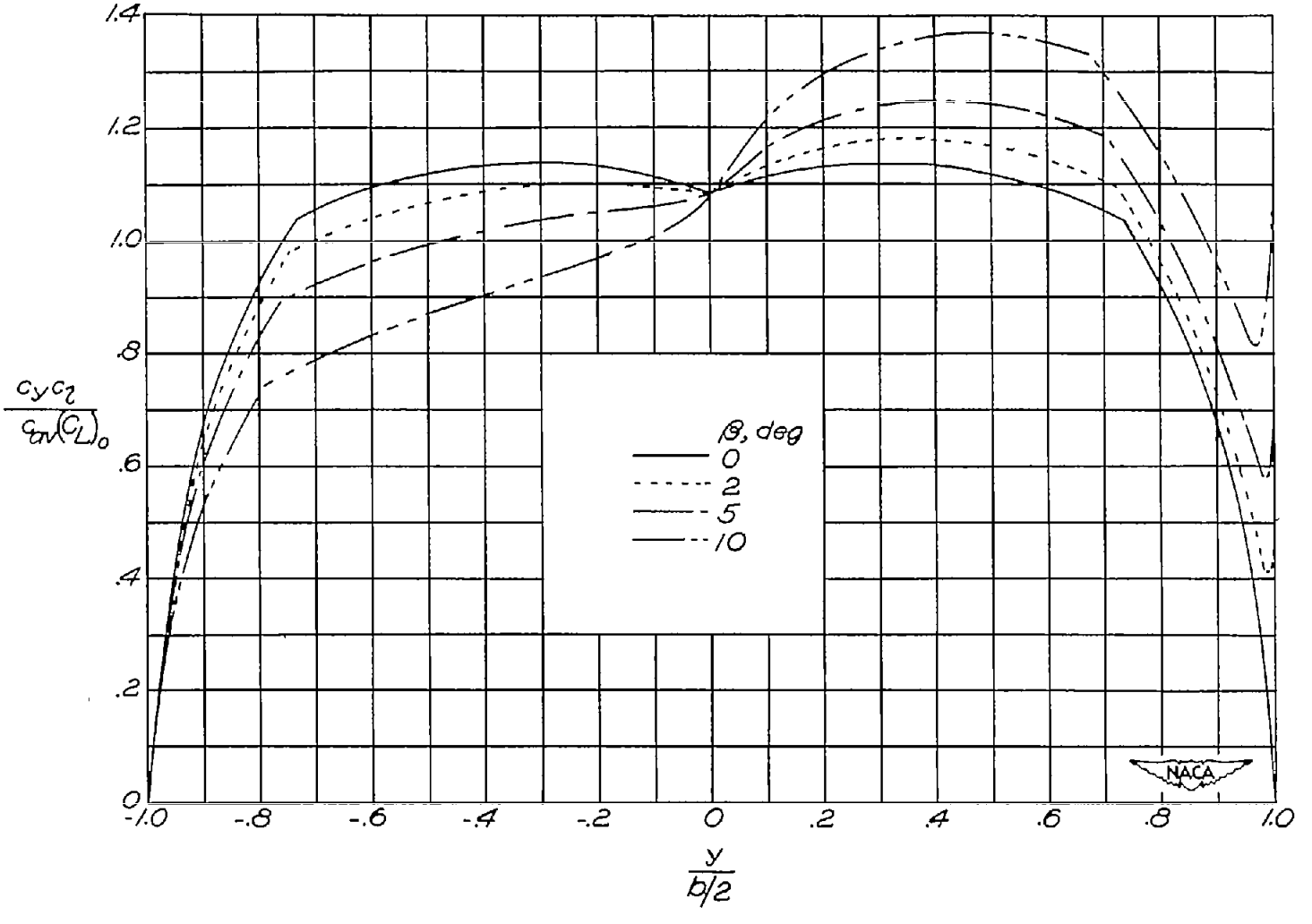

(b) $\lambda = 0.25$; $M = 1.4$.

Figure 7.- Continued.

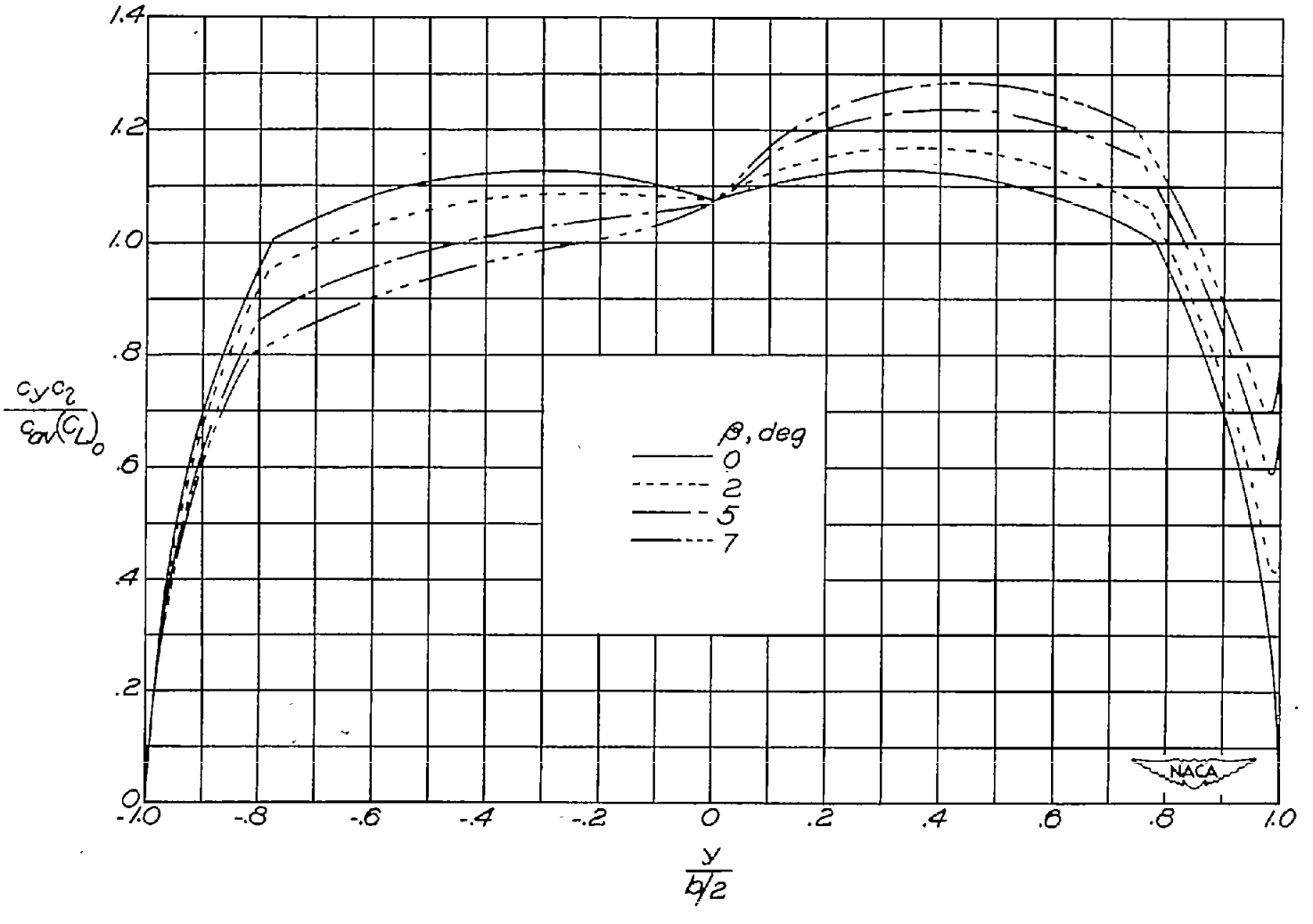

(c) $\lambda = 0.25$; $M = 1.6$.

Figure 7.- Continued.

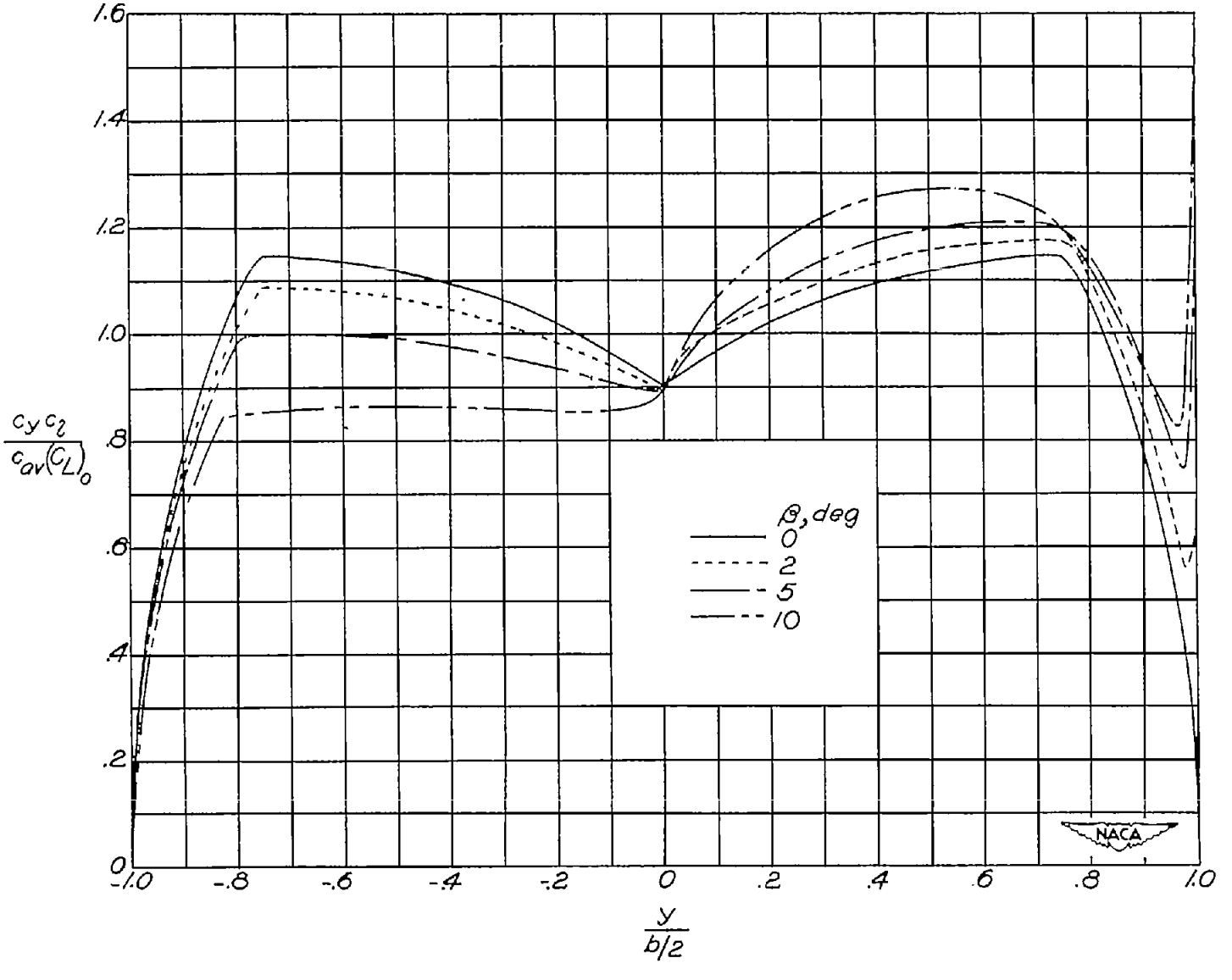

(d) $\lambda = 0.50$; $M = 2.0$.

Figure 7.- Continued.

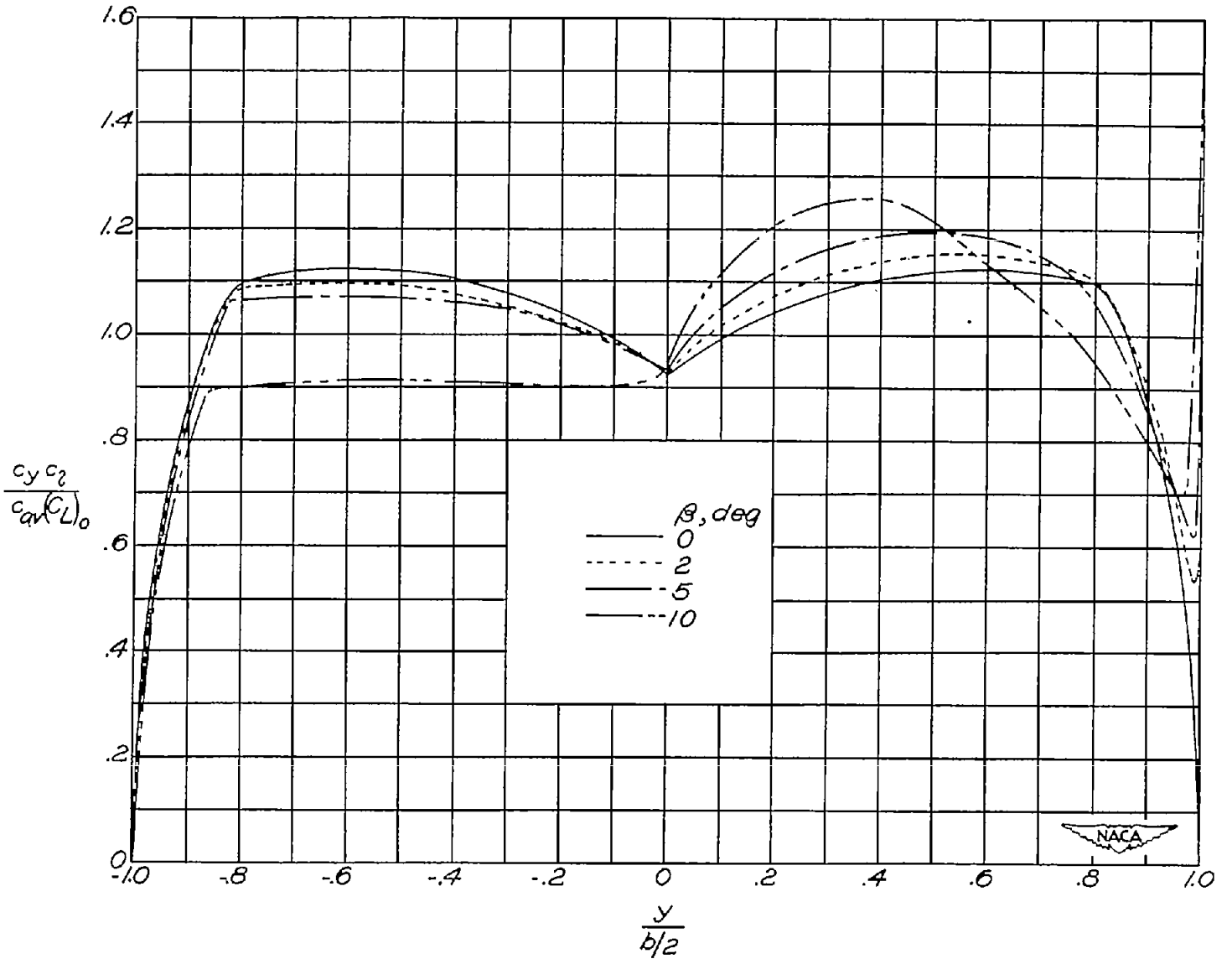

(e) $\lambda = 0.50$; $M = 2.4$.

Figure 7.- Continued.

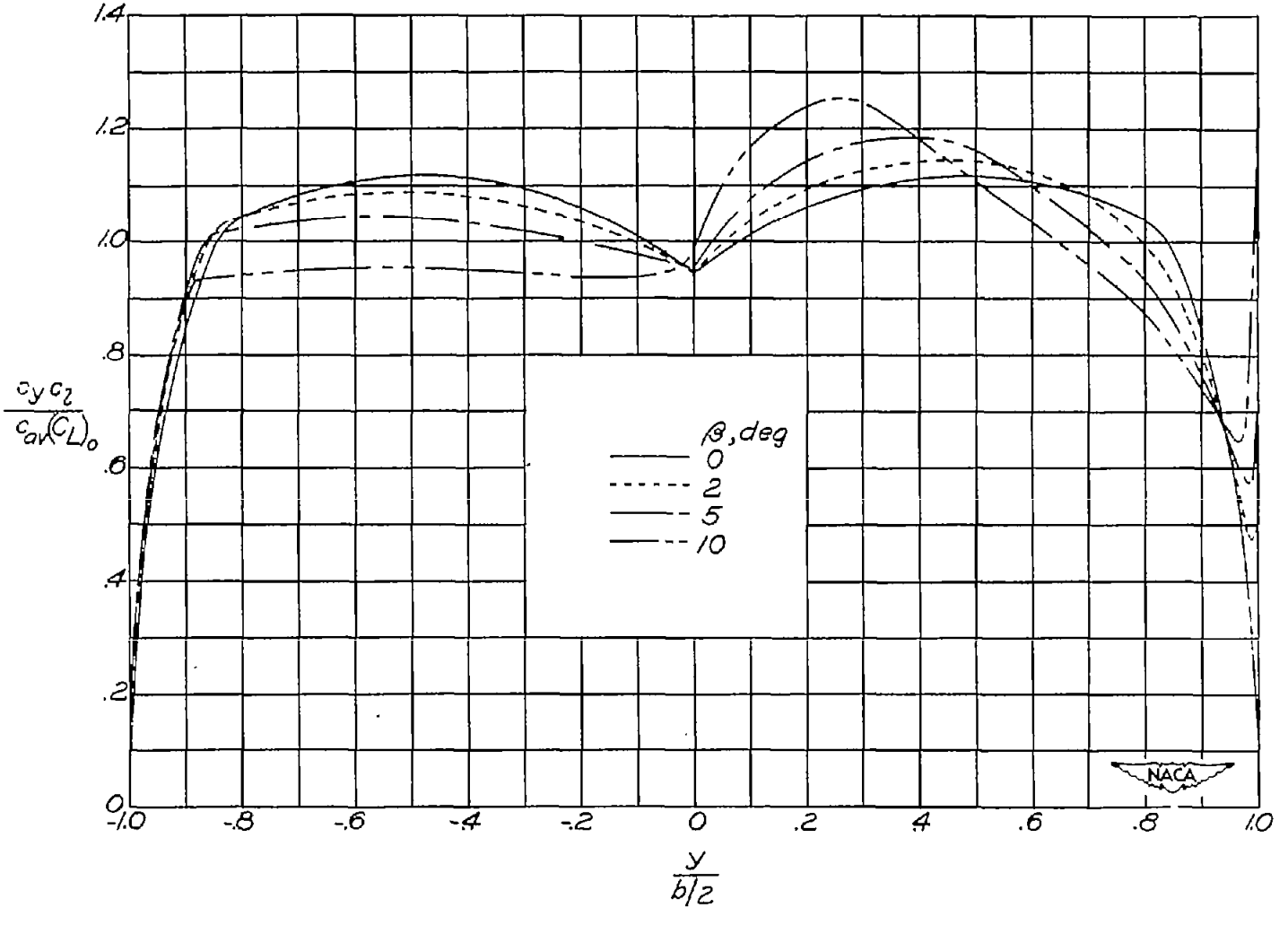

(f) $\lambda = 0.50$; $M = 2.8$.

Figure 7.- Continued.

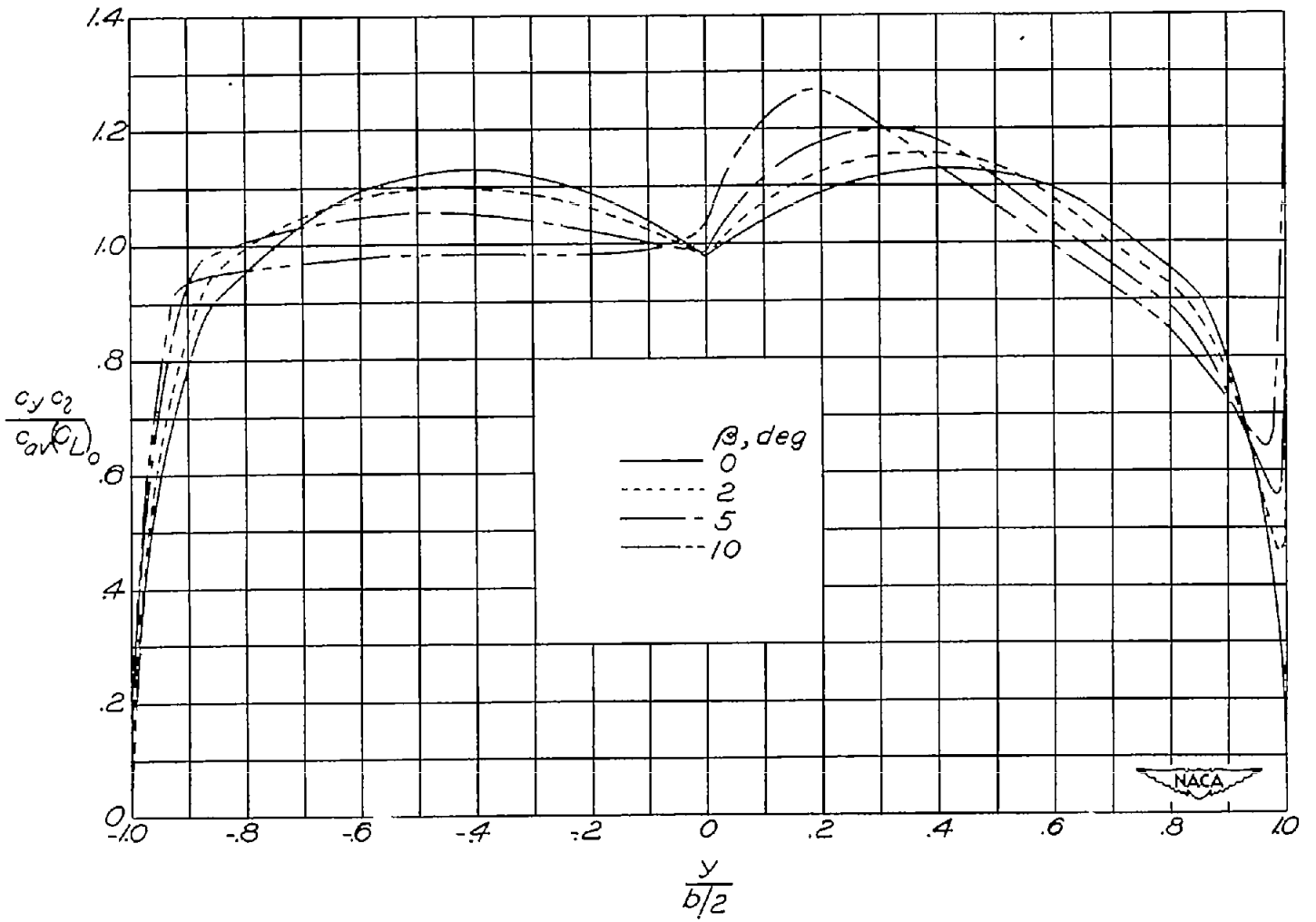

(g) $\lambda = 0.50$; $M = 3.2$.

Figure 7.- Concluded.

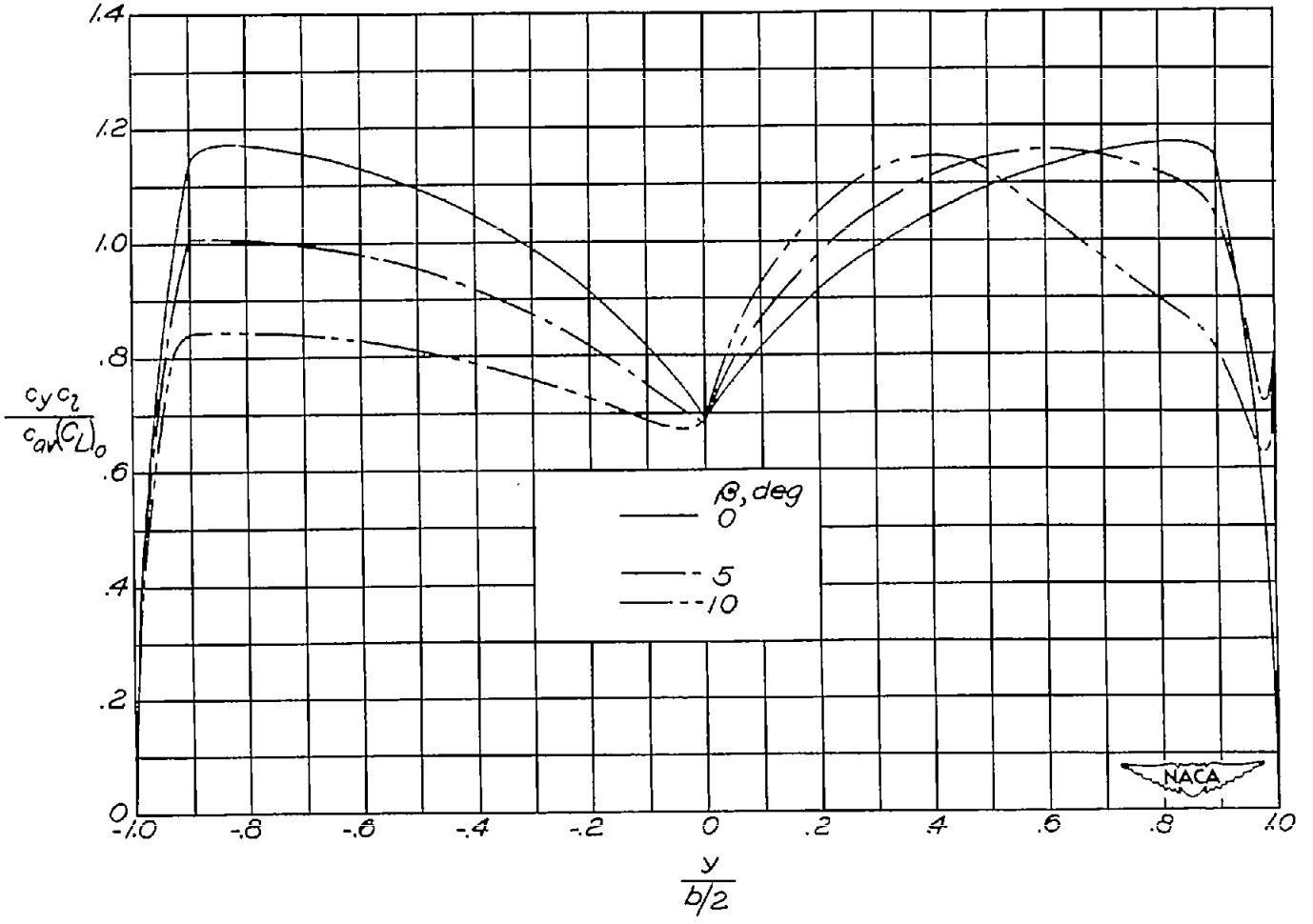

(a) M = 2.0.

Figure 8.- Span loadings at various sideslip angles. $\Lambda = 60^\circ$; $\lambda = 0.50$; $A = 4.0$.

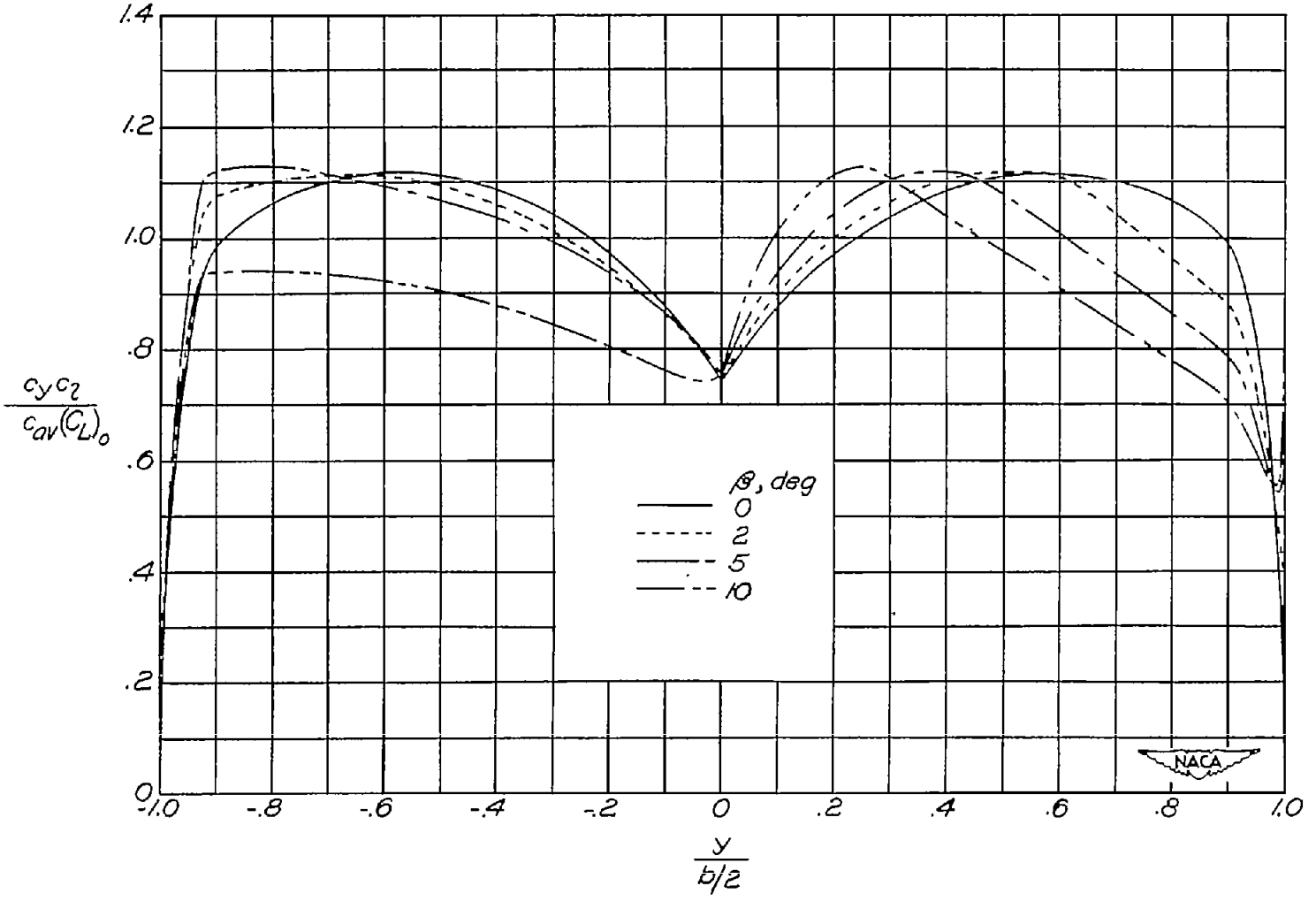

(b) M = 2.4.

Figure 8.- Continued.

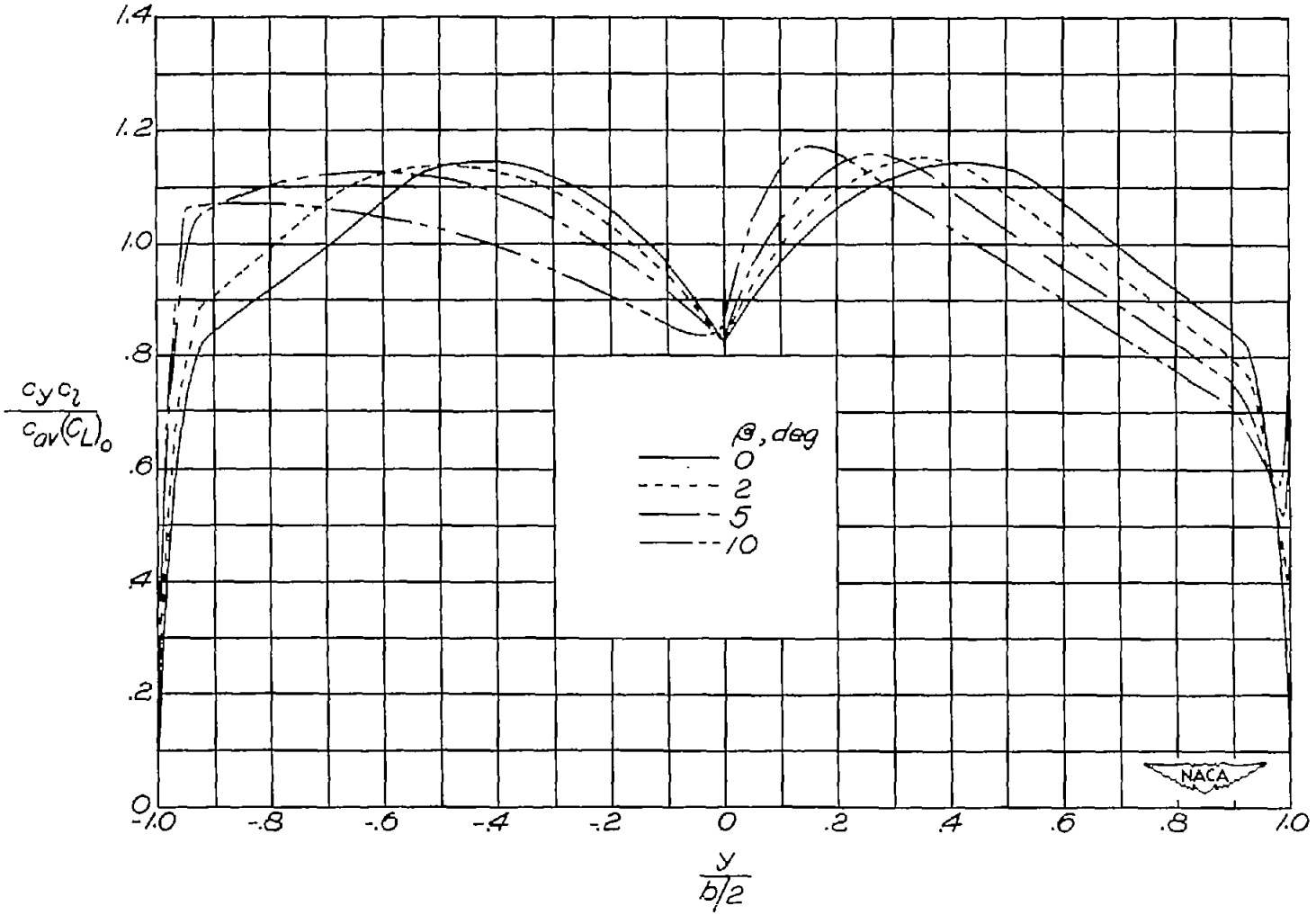

(c) M = 2.8.

Figure 8.- Continued.

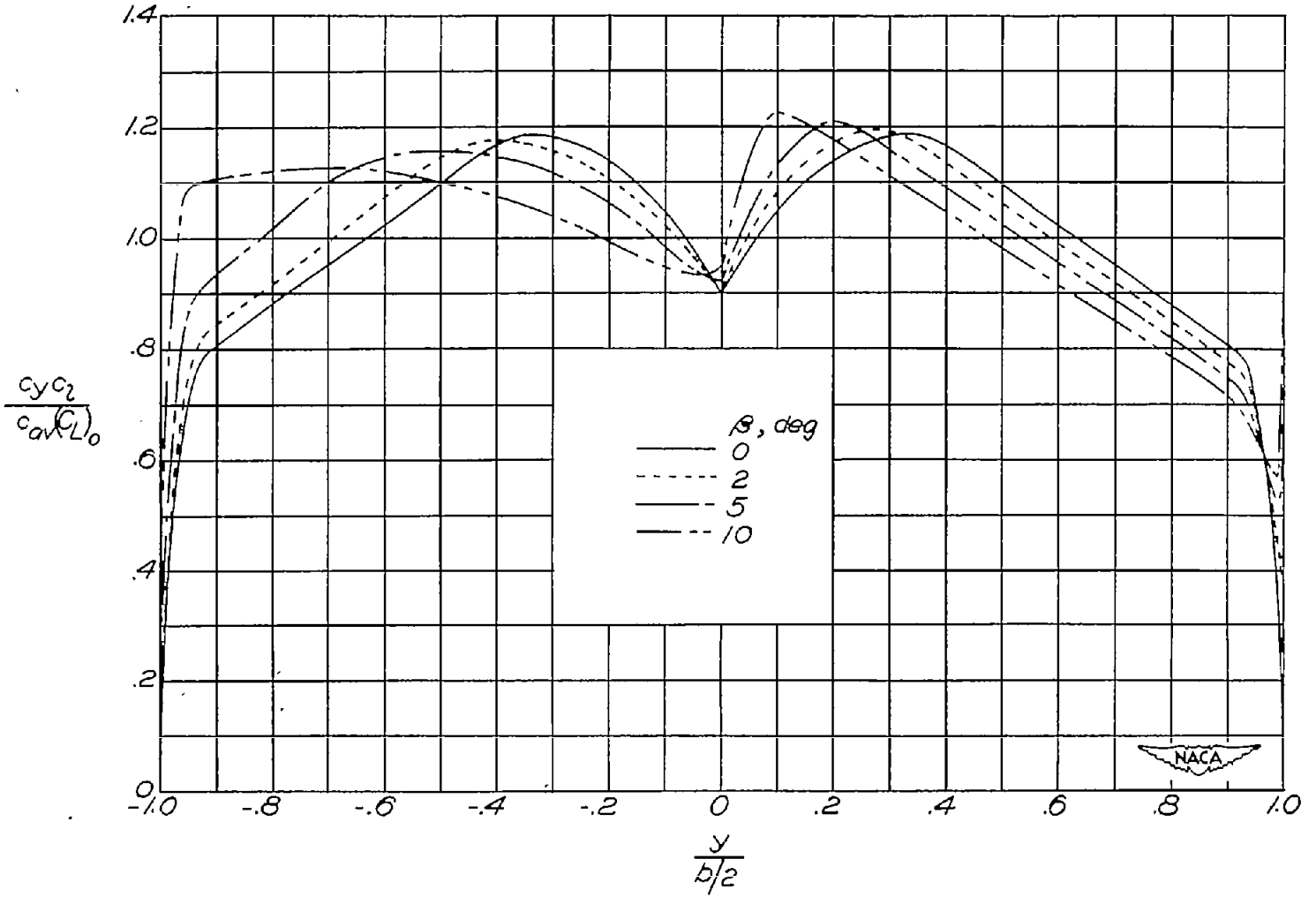

(d) M = 3.2.

Figure 8.- Concluded.

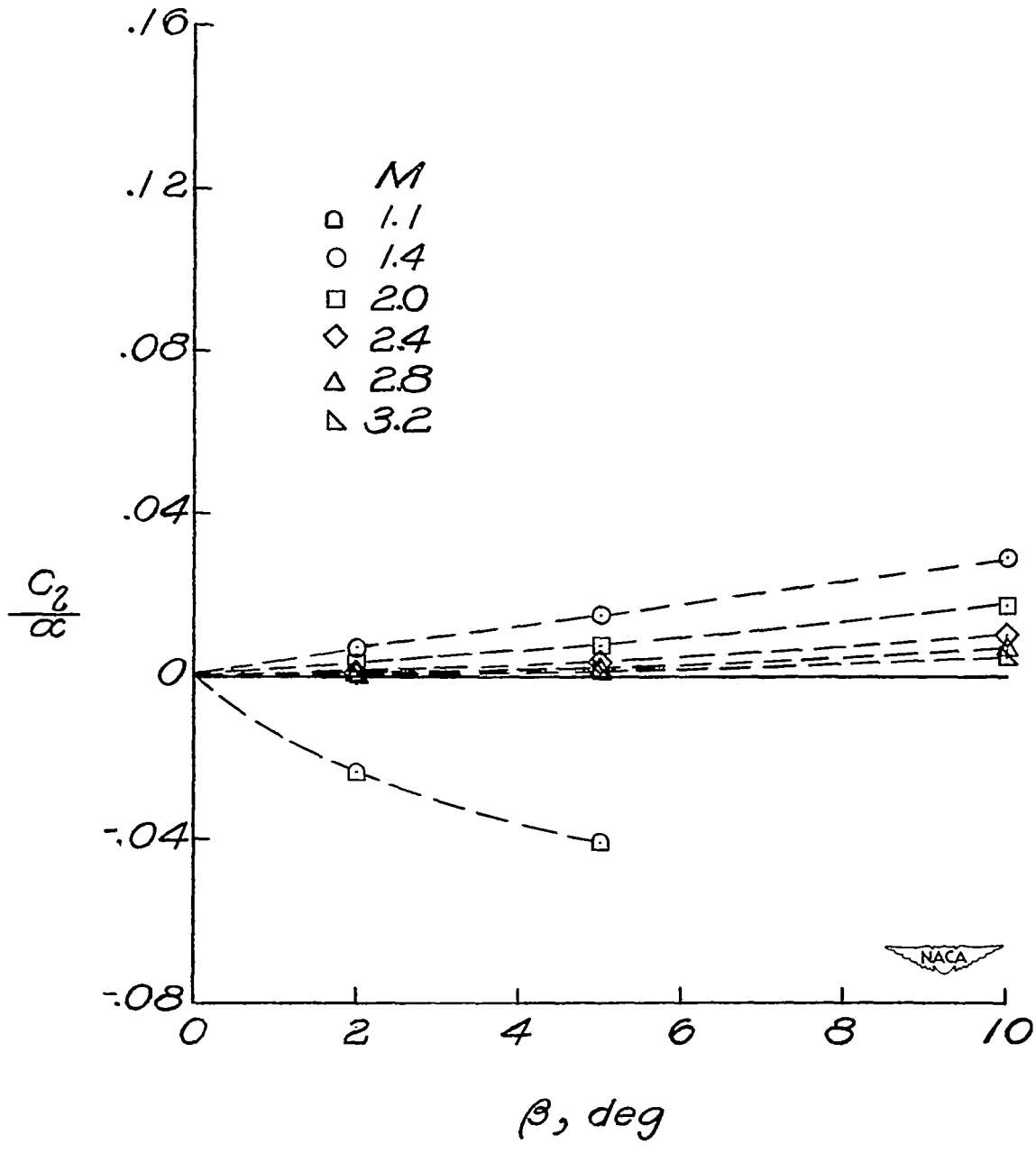

Figure 9.- Variations of the rolling-moment coefficient with sideslip angle for several Mach numbers. $\Lambda = 30^\circ$; $A = 4.0$; $\lambda = 0.5$. Computed points are indicated by appropriate symbols.

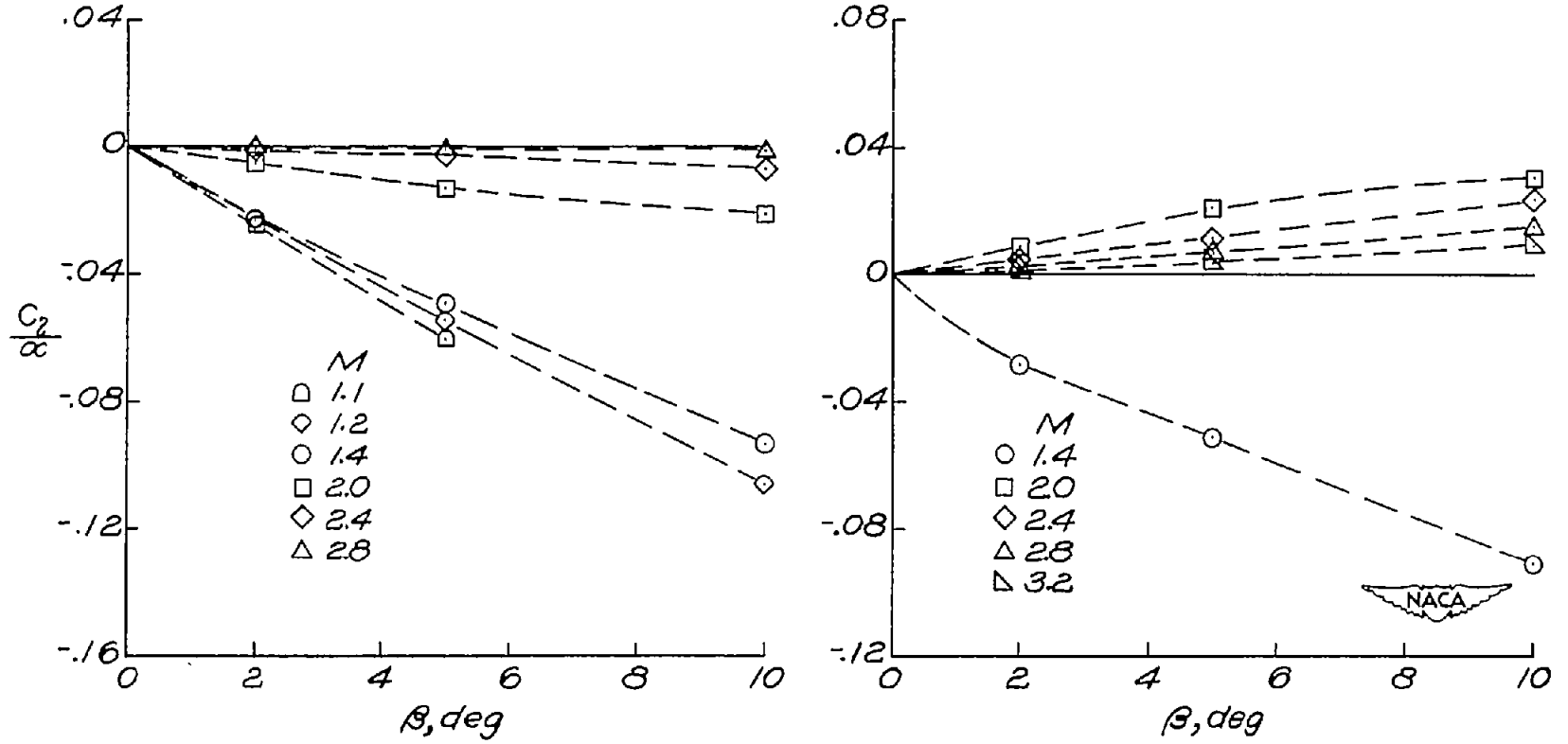

(a) A = 2.0.

(b) A = 4.0.

Figure 10.- Variations of the rolling-moment coefficient with sideslip angle for several Mach numbers. $\Lambda = 45^\circ$; $\lambda = 0.5$. Computed points are indicated by the appropriate symbols.

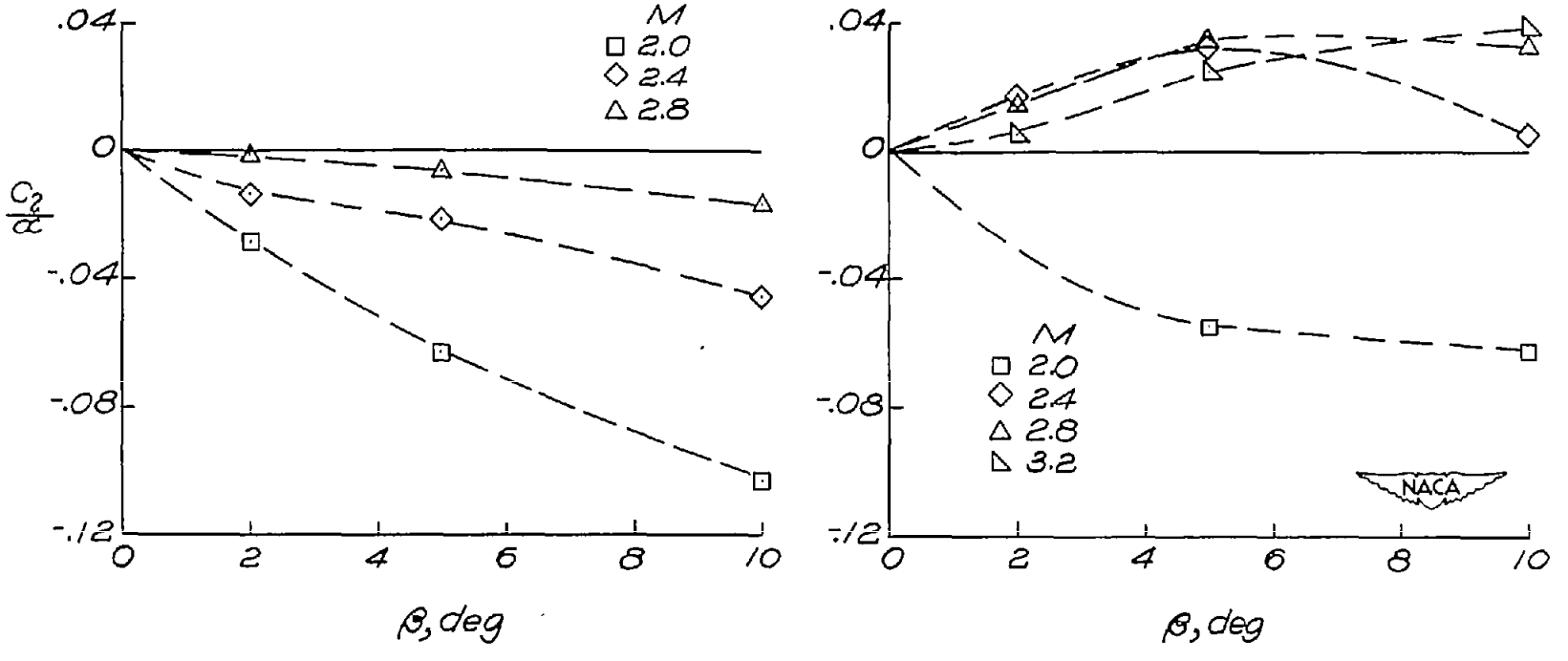

(a) A = 2.0. (b) A = 4.0.

Figure 11.- Variations of the rolling-moment coefficient with sideslip angle for several Mach numbers. $\Lambda = 60°$; $\lambda = 0.5$. Computed points are indicated by the appropriate symbols.

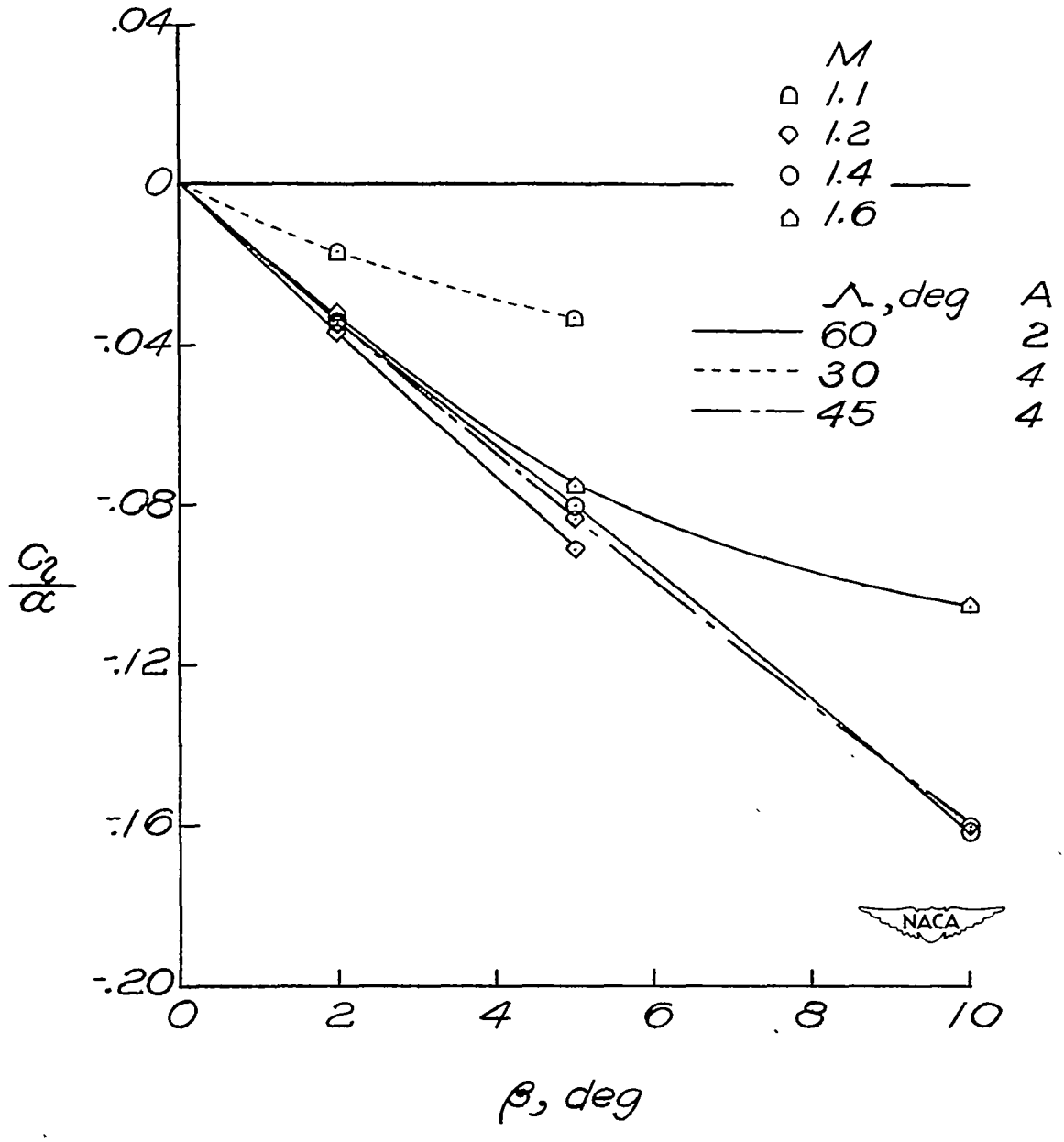

Figure 12.- Variations of the rolling-moment coefficient with sideslip angle for several Mach numbers and for various plan forms with taper ratio 0.25. Computed points are indicated by the appropriate symbols.

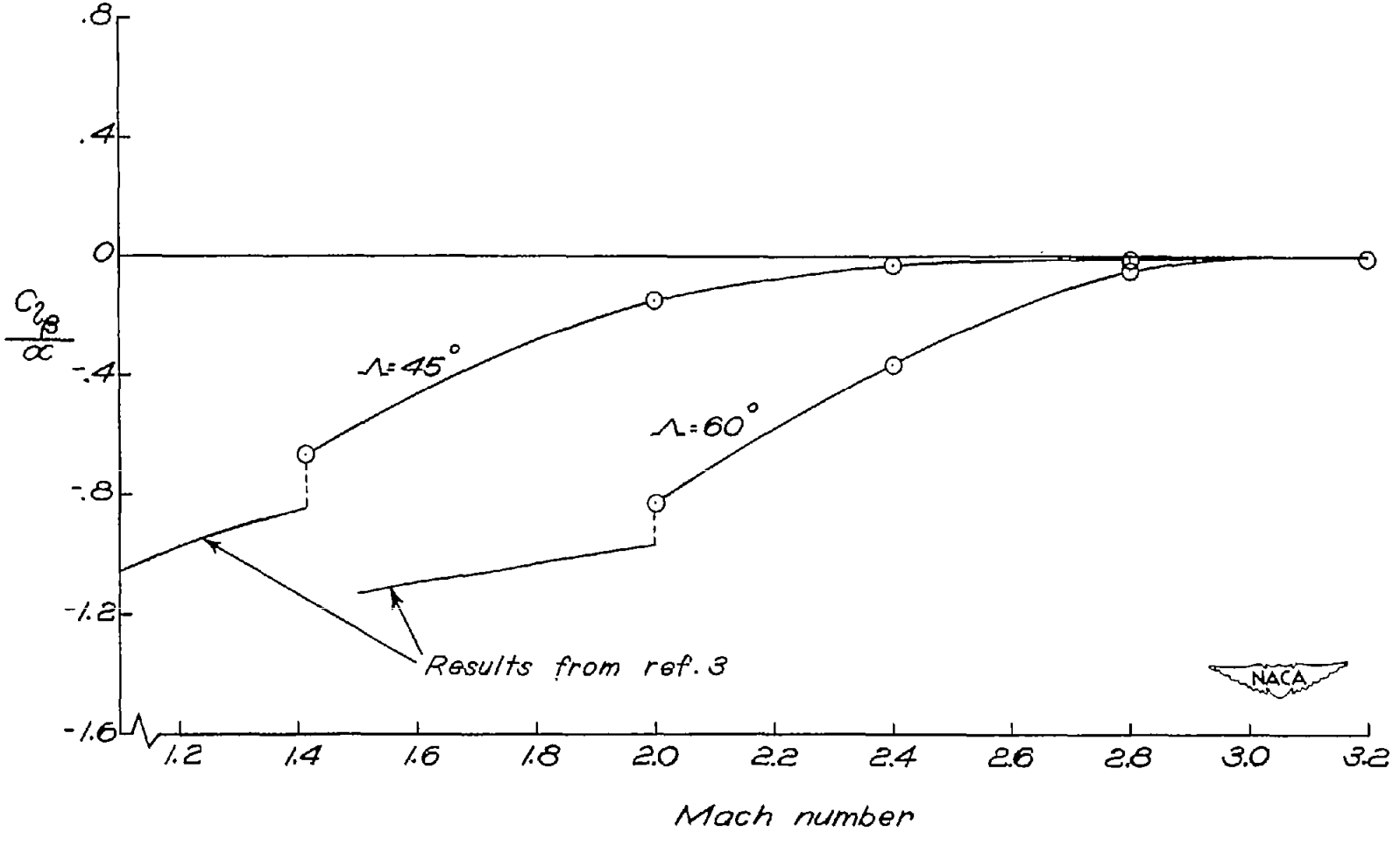

Figure 13.- Variations of the stability derivative C_{l_β} with Mach number for wings of aspect ratio 2.0 and taper ratio 0.5. Computed points are indicated by circles. (Results are valid for both body and stability systems of axes.)

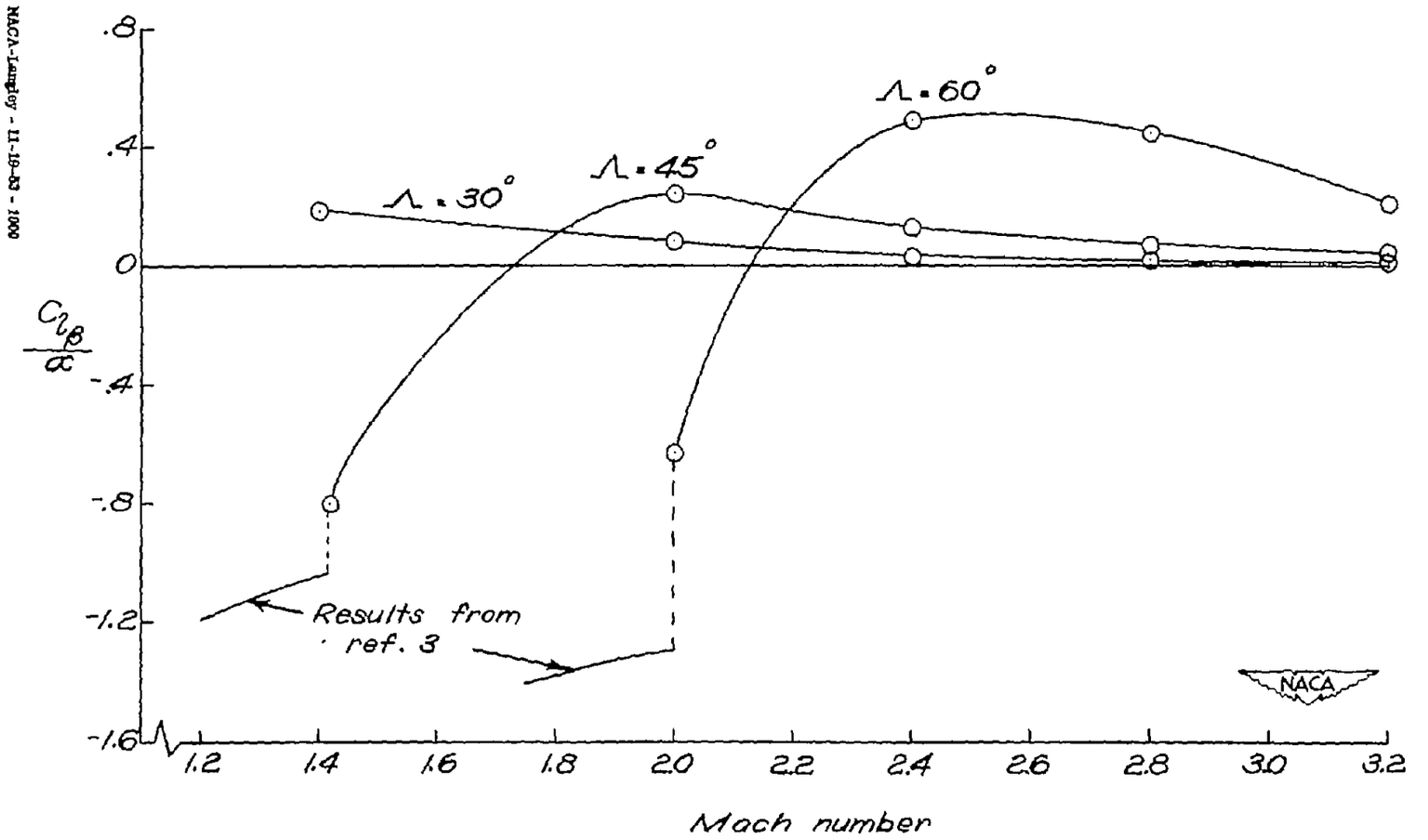

Figure 14.- Variations of the stability derivative C_{l_β} with Mach number for wings of aspect ratio 4.0 and taper ratio 0.5. Computed points are indicated by circles. (Results are valid for both body and stability systems of axes.)